Hindawi
Geofluids
Volume 2021, Article ID 6671871, 22 pages
https://doi.org/10.1155/2021/6671871

Review Article

CO_2-Fluid-Rock Interactions and the Coupled Geomechanical Response during CCUS Processes in Unconventional Reservoirs

Mingyu Cai, Yuliang Su, Lei Li, Yongmao Hao, and Xiaogang Gao

School of Petroleum Engineering, China University of Petroleum, Qingdao 266580, China

Correspondence should be addressed to Mingyu Cai; b17020068@s.upc.edu.cn and Yuliang Su; suyuliang@upc.edu.cn

Received 26 November 2020; Revised 12 January 2021; Accepted 15 February 2021; Published 26 February 2021

Academic Editor: Julie Pearce

The difficulty of deploying remaining oil from unconventional reservoirs and the increasing CO_2 emissions has prompted researchers to delve into carbon emissions through Carbon Capture, Utilization, and Storage (CCUS) technologies. Under the confinement of nanopore in unconventional formation, CO_2 and hydrocarbon molecules show different density distribution from in the bulk phase, which leads to a unique phase state and interface behavior that affects fluid migration. At the same time, mineral reactions, asphaltene deposition, and CO_2 pressurization will cause the change of porous media geometry, which will affect the multiphase flow. This review highlights the physical and chemical effects of CO_2 injection into unconventional reservoirs containing a large number of micro-nanopores. The interactions between CO_2 and in situ fluids and the resulting unique fluid phase behavior, gas-liquid equilibrium calculation, CO_2 adsorption/desorption, interfacial tension, and minimum miscible pressure (MMP) are reviewed. The pore structure changes and stress distribution caused by the interactions between CO_2, in situ fluids, and rock surface are discussed. The experimental and theoretical approaches of these fluid-fluid and fluid-solid reactions are summarized. Besides, deficiencies in the application and safety assessment of CCUS in unconventional reservoirs are described, which will help improve the design and operation of CCUS.

1. Introduction

At present, conventional oil and gas production is decreasing over the years, and the unconventional oil and gas resources, which with rich reserves, have attracted more and more attention. The past decade has seen breakthroughs in North American shale oil development with horizontal wells' maturity and large-scale hydraulic fracturing. The successful development of unconventional resources has transformed the world's energy landscape. Despite advanced horizontal well drilling technology and volume fracturing technology, shale oil's primary recovery is extremely low (~5%-10). The low recovery is mainly because the adsorbed and dissolved crude oil in the shale reservoir cannot be effectively utilized in the primary development [1]. Simultaneously, clay expands when surfactant and water are injected, and the resulting decrease in permeability may make it challenging to increase reservoir pressure [2]. Researchers experimentally compared the effects of CO_2 Huff-n-Puff and water injection on the enhanced recovery of shale oil. The results show that under different shale properties, CO_2 Huff-n-Puff can increase the recovery rate by ~50% (from 33% to 85%), and the overall effect is far better than that of surfactant and water injection [3]. Compared with the injection of other miscible gases such as N_2 and CH_4, CO_2 has lower minimum miscibility pressure (MMP), resulting in more extensive oil expansion, more viscosity reduction, and mobility improvement. Adsorbed oil can also be effectively used through extraction [4]. CO_2 injection has become one of the potential means of developing unconventional resources efficiently.

Simultaneously, the coupling of scientific and engineering issues with social and political discussions concerns the challenges posed by the harmonious coexistence of energy, climate, and environment. Another research topic that arises is reducing carbon emissions through Carbon Capture, Utilization, and Storage (CCUS) technologies. Over half of the top 10 largest CO_2 storage projects counted in 2019 transported the captured CO_2 by pipeline to nearby oilfields to enhance gas/oil recovery. The Century Plant and Shute Greek Gas Processing Plant projects, which ranked first and second

worldwide, have unconventional reservoirs as their primary storage sites. The CO_2 from Century Plant is for use in EOR projects in the Permian Basin. It is expected to use at least 3.5 trillion cubic feet of CO_2 in Avalon shale, Bone Spring, Wolfbone/Wolfcamp, Cline shale, Wolfberry, and Delaware to develop approximately 500 million barrels of reserves from currently owned assets at an attractive cost. The Rangely Weber unit in Salt Creek field, one of the storage sites for Shute Greek Gas Processing Plant, is the world's largest extralow permeability sandstone reservoir developed by CO_2-WAG miscible flooding [5]. China has included CCUS in its latest five-year economic development plan, is building large-scale carbon storage facilities, and provides financial support for CCUS pilot projects. Notable examples of the developments over the past decade include the CCUS facility in PetroChina Jilin Oil Field, Changqing Oil Field, and Sinopec Zhongyuan [6].

Successful application of CO_2 enhanced recovery (EOR) technology and its storage in unconventional reservoirs requires a comprehensive understanding of CO_2-fluid-rock interactions, incredibly nanoscale fluid-rock interactions that play an essential role in unconventional formations. Possible interactions in the reservoir within injected CO_2 have been central to the system's overall evolution in dissolution, precipitation, secondary mineral formation, and deposition. This paper mainly reviews the in situ fluid between CO_2 and reservoir brine, and crude oil and the physical and chemical reactions between CO_2 and reservoir minerals. The pore size changes, connectivity, and reservoir stress distribution caused by fluid-fluid and fluid-solid reactions are also summarized. Finally, the future research directions and challenges for the research and application of CO_2-CCUS are discussed.

2. CO_2-Oil Interactions and Phase Behaviors

2.1. Adsorption and Desorption. As early as the beginning of the last century, it had been established that fluids could adsorb on solid surfaces [7], and this phenomenon was also confirmed in subsequent studies [8, 9]. In conventional reservoirs, pores are measured in millimeters. In such porous media with relatively large pore size, fluid adsorption is usually negligible. However, when the pore size in the shale is nanoscale (1-100 nm), the pore space occupied by the adsorbed fluid can no longer be ignored due to the increase of the specific surface area pore. Although there have been many studies on oil and gas adsorption, the performance of the mixture in unconventional reservoirs is still a challenging research topic due to the complex conditions caused by multicomponent fluids, high temperature, high pressure, and heterogeneous pore distributions in reservoirs.

In terms of experiments, microfluidic technology development makes it possible to measure the PVT parameters of multiphase fluids quickly. Molla and Mostowfi [10] completed the PVT test of reservoir fluids in a wide range of <86 MPa and <150°C by making a curved narrow single-capillary channel model. Rapoport et al. [11] carried out a two-phase flow experiment using a microfluidic model and pointed out that the phase interface can promote two-phase fluid's simultaneous motion. Karadimitriou et al. [12] observed two-phase distribution characteristics in quasistatic displacement and imbibition and measured the phase saturation and interface area. Another factor to consider is the strong interaction between CO_2 and organic matter. The injected CO_2 hydrocarbon fluids are competitive for adsorption in porous media. Chareonsuppanimit et al. [13] carried out CH_4, CO_2, and N_2 adsorption experiments on shale and coal and found that the adsorption amount of these gasses on shale was lower than that of coal with the same maturity. Zhang et al. [14] conducted competitive adsorption experiments on shale sing CO_2-CH_4 binary gas and showed that the separation coefficient would decrease with CO_2 concentration. Bergaoui et al. [15] confirmed that the adsorption n-alkane series, C_1–C_7, on activated carbon was much different because of the distinct molecules' sizes. Although the above works are of guiding significance for the competitive experiments, they are mostly focusing on the interactions between CO_2 and light components with short molecular chain length.

Some studies on the simulation of oil/gas adsorption in unconventional reservoirs can be seen in recent years. Molecular simulation studies have predicted the density distribution of methane in slit nanopores [16]. The results showed that methane is adsorbed on the graphite pore wall with a size of 1.14-3.93 nm at the reservoir temperature (353 K) and pressure (21 MPa). Studies of the behavior of binary mixtures (C_1/C_2 and C_1/C_3) using the Grand Canonical Monte Carlo (GCMC) method have found that heavier hydrocarbon components are more likely to stay in the adsorbents [17]. The adsorption of methane in activated carbon was highly sensitive to the pore size. When both micropores and mesopores were present, the maximum methane excess adsorption in the micropores (0.4 nm) was ten times (about 12.5 times) higher than that in the mesopores (9 nm) [18]. These molecular simulations refine the results of studies on the behavior of hydrocarbon components in porous media. However, the computation-intensive property limits the molecular scale simulations at a large scale (>100 nm). Simultaneously, the extensive application of CO_2 in unconventional oil/gas development brings new research topics. Zeng et al. [19] claimed that CO_2 did not form an apparent single adsorption layer in kerogen in organic nanopores. They pointed out that it was more reasonable to use the improved BET model for the adsorption amount. CO_2 has a robust competitive adsorption capacity for hydrocarbon components of shale oil. The selective adsorption capacity is comprehensively affected by reservoir temperature and pressure, kerogen type and maturity, water content, and pore surface wettability. Liu et al. [20] investigated the competitive adsorption of CO_2-C_1-C_4 mixtures in the double pore system with 1 nm and 3 nm of pore sizes (Figure 1(a)). The above results mainly focus on the competitive adsorption of CO_2 and lighter components in shale. Concerning the heavier components (n-alkane), simulation results indicated that CO_2 replaced the adsorbed hydrocarbons on the surface of calcite, and the amount of adsorbed CO_2 is controlled by the number of calcium potential on pore surfaces (Figure 1(b)) [21]. With the increase of CO_2 composition, CO_2 can mix with hydrocarbons in other

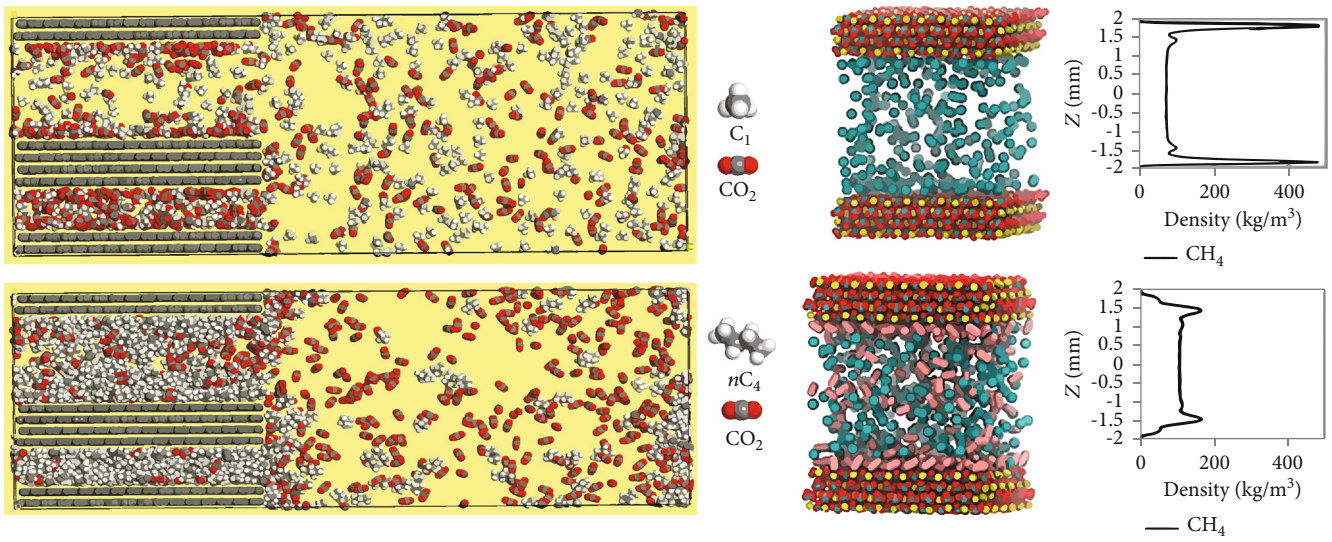

(a) Adsorption in graphene double-nanopore system

(b) Adsorption in calcite nanopores

FIGURE 1: CO_2 adsorption in organic (a) [20] and inorganic (b) [21] pores.

pore areas only after the surface's adsorption layer is entirely saturated. Besides, temperature, pore size, CO_2 fraction, and length of n-alkanes are key factors in the selective adsorption of CO_2 and n-alkanes [21]. In general, the microscopic interaction mechanism between CO_2 and n-alkanes, such as octane and decane, has been rarely reported.

2.2. Phase Behavior of Confined Fluids. Due to the significant portion of nanopores in such formations' total pores, the study of the influence of nanopores on the phase behavior of a single component and mixture is of great importance for improving oil and gas recovery in unconventional tight/-shale reservoirs. As early as the 1960s, the effect of pore size on fluid properties has been known, and the relationship between phase behavior and pore size in porous media has been studied through physical experiments. Here, the results of phase behavior experiments over the past 60 years (Table 1) are summarized. It is found that the saturation pressure of pure components in nanopores is usually decreased significantly under a specific temperature. The critical temperature and pressure shifts occur with pore diameter decrease to the nanoscale. The hydrocarbon mixture phase sees a decrease in the bubble point pressure and upper dew point pressure and an increase in the lower dew point pressure. The shifts in vapor and liquid equilibrium (VLE) are also related to molecular chain length, wetting film, pore size, and microporosity. With the development of CO_2-EOR and the increasing application of CO_2 storage in low pressure or depleted oil/gas field, more and more studies began to investigate capillary condensation of CO_2-hydrocarbon mixtures confined in nanometer porous media.

Microfluidics visualization technology has advantages in speed, control, and sample size and can provide phase characterization analysis similar to existing batch methods. In contrast, nanofluids (<100 nm) provides unique insight into nanoscale phase transition phenomena. However, experiments often cost a lot to get inadequate data. Although powerful, imaging tools still do not understand the basic mechanisms by which fluids reside and flow in nanopores. Therefore, theoretical research has attracted more and more attention in recent years. Methods such as molecular dynamics (MD) simulation and density functional theory (DFT) have proved to be powerful tools for studying confined fluids' local properties. Grand canonical Monte Carlo simulation can be used to study the effects of confinement on adsorption, capillary condensation, and freezing/melting of fluids in nanopores [36]. Density functional theory (DFT) and mean-field approximation have been used to study the effects of nanoconfinement on fluids' thermodynamic properties. Based on the simulation results, a model was proposed to predict the adsorption of nonpolar and polar binary mixtures, and the relative contributions of fluid-wall and fluid-fluid interactions were analyzed [37]. In applying nonlocal density functional theory (NLDFT), the pores of nitrogen and argon condense/evaporate in mesoporous molecular sieves (MMS) with cylindrical channels. The Lennard-Jones potential is used to consider the interaction potential between fluid and solid-fluid molecules. The prediction of adsorption/desorption isotherms by this model is in good agreement with the experimental data, but there is a significant deviation in pores less than 5 nm [38]. Using the Gibbs Ensemble Monte Carlo (GEMC) NVT instead of the traditional Grand Regular Monte Carlo Ensemble (GCMC) simulation to study the pure components (including methane, ethane, pentane, and n-decane) can avoid limitations to determine the phase transition location. In this way, a more accurate equilibrium pressure of liquid and gas can be obtained. GEMC-NPT-BPM (Bubble point Monte Carlo) was developed in conjunction with GEMC NVT simulations to obtain thermodynamic properties [39], including confined equilibrium pressure for the mixture. The simulation results show the shifts and closure of the confined fluid phase envelope relative to the bulk fluid. The critical temperature and pressure transfer to lower than the bulk value, the bubble

Table 1: Literatures study on confined phase behavior experiments.

References	Pore sizes	Fluids	Results
Tindy and Raynal [22]	$g_s = 160 - 200$ μm	Oil samples, methane, and n-heptane	P_b is higher in the porous medium than the PVT cell. But there is no difference for a mixture of methane and n-heptane.
Trebin and Zadora [23]	$d_p = 0.3 - 0.215$ mm	Gas condensate	P_d is 10% to 15% higher with a larger surface area. Higher temperature reduces the effect of porous media on VLE.
Sigmund et al. [24]	/	C_1-nC_4 and C_1-nC_5 mixtures	High surface curvatures lead to lower P_b.
Thommes and Findenegg [25]	$d_p = 24 - 31$ nm	SF6	T_c shifts in slit-like and circular nanopores are observed.
Findenegg et al. [26]	$d_p = 7.7 - 24$ nm	Cyclopentane, isopentane, and perfluoropentane	Decreases in critical temperatures are observed.
Voronov et al. [27]	$d_p = 2.3$ μm	Methane and n-pentane mixtures	The shifts of P_d and P_b are caused by the wetting film on the pore surface.
Qiao et al. [28]	$d_p = 2.40 - 4.24$ nm	Hexane	With increased temperature and pore size, the phase transition step's position shifts to higher relative pressure.
Vinh-Thang et al. [29]	$d_p = 4.6 - 7.8$ nm	n-Heptane and toluene	Adsorption isosteric heat is found to depend on the microporosity of porous media.
Zeigermann et al. [30]	$d_p = 6 - 15$ nm	n-Pentane	Fluid changed from liquid to supercritical state even under measured T_c.
Russo et al. [31]	$d_p = 3.54 - 30.47$ nm	Toluene, methylcyclohexane, neopentane, and n-pentane	The isosteric enthalpies associated with capillary condensation are higher than the molar condensation enthalpies in smaller pores.
Luo et al. [32]	$d_p = 4.3, 38.1$ nm	Octane, decane, and the binary mixture	Two distinct bubble points are observed at 4.3 nm, suggesting two populations of evaporating fluid.
Barsotti et al. [33]	$d_p = 2.9, 4.19$ and 8.08 nm	Propane, n-butane, and n-pentane	Pressure phenomena of the confined fluids are different due to the molecular chain lengths of the adsorbates.
Tan et al. [34]	$d_p = 4.570, 6.079$ and 8.145 nm	CO_2 and ethane	The presence of the critical point confined in nanopores is demonstrated and measured for the first time.
Qiu et al. [35]	$d_p = 2.4 - 200$ nm	CO_2, ethane, and n-hexane	After the bulk liquid is completely evaporated, confined fluids then evaporate at a higher temperature or at a lower pressure than that in bulk space.

point pressure decreases, and the dew point pressure increases. The adsorption of heavier components in methane/ethane and ethane/n-pentane mixtures increased in the vapor phase due to the nanopore walls' effect, and correspondingly, the adsorption of lighter components increased in the liquid phase. However, their applicability is limited to more complex problems, such as the spatial distribution of fluid mixtures in heterogeneous porous matrices due to their computational complexity.

2.3. Modified EOS and VLE Calculation. It is impossible to study the distribution of fluid mixture in large-scale heterogeneous porous matrix by molecular-scale calculation. Therefore, researchers have focused on developing analytical (semiempirical) EOS models. An equation of state (EOS) in thermodynamic is an equation that provides the relations between temperature, pressure, volume, and some other variables. There are many different forms of cubic EOS in the literature. The van der Waals, back in 1873, introduced the first cubic EOS that was derived by the assumption of a finite volume occupied by the constituent molecules [40]. Based on van der Waals EOS, many other cubic EOS were derived [41–45], among which the Peng-Robinson (PR) EOS and the Soave-Redlich-Kwong (SRK) EOS are the most two widely used forms of EOS in the petroleum industry. However, although good prediction results can be obtained under specific temperature and pressure conditions, these cubic EOS are all in the assumption that the fluids are in bulk systems without boundary effects or restrictions. To better predict the hydrocarbon phase behavior in porous media, researchers suggest the conventional EOS should be modified to consider the wall forces' existence and the competition between the fluid-fluid and fluid-wall interactions of confined fluids.

In some of the earliest work, the researchers coupled capillary pressure effects to two-phase equilibria of hydrocarbon mixtures to meet unconventional reservoirs' nonnegligible capillary forces [46]. Tsallis [47, 48] proposed to extend vdW EOS to predict critical temperature shifts with pore size qualitatively and quantitatively. Some subsequent studies apply vdW equations to the fluid calculation in slit-like pores based on perturbation theory [49]. In the calculation using the proposed new equation of state (EOS) incorporating capillary pressure, both bubble and dew point pressures are compared to experimental and molecular simulation results. Moreover, there is a maximum capillary pressure at each temperature beyond which equilibrium cannot be reached [50]. However, most of the predictions are not ideal when

approaching the critical point. Equation (1) describes two-phase flash evaporation under capillary pressure.

$$\begin{gathered} P_V - P_L = P_{\text{cap}} = \frac{2\delta \cos \alpha}{r_p}, \\ f_L^i(T, P_L, x) = f_V^i(T, P_V, y), \quad i = 1, \cdots, N_c, \\ f_L^i(T, P_L, x) = \varnothing_{iL} x_i P_L, \\ f_V^i(T, P_V, y) = \varnothing_{iV} y_i P_V. \end{gathered} \tag{1}$$

Apart from merely adding capillary pressure, researchers have obtained the critical shifts of confined fluids by combining molecular simulation, DFT, and experimental data. One of the results of the investigation was the approximation described in Equation (2).

$$\frac{T_c - T_{\text{cp}}}{T_c} \backsimeq \frac{\sigma_{\text{LJ}}}{r_p}. \tag{2}$$

The effects of temperature on isothermal adsorption for Ar, N_2, O_2, C_2H_4, and CO_2 in mesoporous were investigated. Moreover, the quantitative relationship between pore size, molecular properties, and criticalities shifts was characterized [51, 52]. The McM-41 sieves are set with the various pore. However, the study is based on classical thermodynamics and ignores the interaction between molecules and pore walls. Moreover, although the simulation results are consistent with the measurement results of capillary condensation, the influence of scale effect on the change process is not well reflected from the change of volume phase to the restricted critical property. Based on the generalized Van der Waals equation of state theory for confined Lennard-Jones fluids in nanopores, a new variation estimation formula for critical attributes is proposed, as shown in Equation (3) [53]. In this proposed correlation, the adsorption and desorption in nanopores are ignored.

$$\begin{gathered} \frac{T_c - T_{\text{cp}}}{T_c} = 0.9409 \frac{\sigma_{\text{LJ}}}{r_p} - 0.2415 \left(\frac{\sigma_{\text{LJ}}}{r_p}\right)^2, \\ \frac{P_c - P_{\text{cp}}}{P_c} = 2 \frac{c_1}{a\sqrt{\pi}} \frac{\sigma_{\text{LJ}}}{r_p} - 2 \frac{c_2}{a\pi} \left(\frac{\sigma_{\text{LJ}}}{r_p}\right)^2, \end{gathered} \tag{3}$$

where $a = 16\pi/9$, $c_1 = 4.6571$, and $c_2 = -2.1185$.

A configurational-bias grand-canonical transition-matrix Monte Carlo simulation was carried out for the critical temperature in smaller nanopores (0.5-5 nm) [54]. This simulation result is summarized as the general correlation between ΔT_c and d_p/σ_{LJ}, as shown in Equation (4). This correlation is widely used in EOS models with shifted critical properties in nanoscale porous media [55–59]. However, lower critical pressures were observed in the following molecular simulation of Lennard-Jones fluids in carbon nanopores with adsorption properties [60, 61].

$$\begin{gathered} \Delta T_c = 0.6, \quad \text{when } \left(\frac{d_p}{\sigma_{\text{LJ}}}\right) < 1.5, \\ \Delta T_c = 1.1775, \quad \text{when } \left(\frac{d_p}{\sigma_{\text{LJ}}}\right) \geq 1.5 \end{gathered} \tag{4}$$

Singh's results were subsequently used to investigate the influence of molecular weight on the critical properties of confined single-component hydrocarbons [56] and the specific changes in phase behavior and critical properties of different hydrocarbon mixtures in the nanospaces [62, 63]. Later, Islam et al. [64] compared the difference in confined phase behavior description within Peng-Robinson EOS and the vdW based on a new proposed correlation. The prediction results of this new relationship are in good agreement with experiments and molecular simulation in the whole range of pore sizes from the scale of single molecule ($\sigma_{\text{LJ}}/r_p \leq 0.5$) to the bulk spaces. The critical terms obtained are

$$\begin{gathered} T_c = \frac{8}{27bR} \left[a - 2{\sigma_{\text{LJ}}}^3 \varepsilon {N_{\text{av}}}^2 \frac{\sigma_{\text{LJ}}}{r_p} \left(c_1 + c_2 \frac{\sigma_{\text{LJ}}}{r_p}\right)\right], \\ P_c = \frac{1}{27b^2} \left[a - 2{\sigma_{\text{LJ}}}^3 \varepsilon {N_{\text{av}}}^2 \frac{\sigma_{\text{LJ}}}{r_p} \left(c_1 + c_2 \frac{\sigma_{\text{LJ}}}{r_p}\right)\right], \\ V_c = 3b. \end{gathered} \tag{5}$$

Furthermore, Travalloni et al. [65] modified PR-EOS (PR-C EOS) by adding terms related to pore size into the equation to influence molecule-wall interactions. Pore size and shape were taken into account in the phase equilibrium calculation. This method can consider the influence of molecular-solid wall interaction energy in different pore sizes and matrix types (heterogeneous adsorbent) when predicting the phase behavior in bulk and confined space.

$$\begin{gathered} P = \frac{RT}{v - b_p} - \psi \sum_{i=1}^{NC} \left(x_i \theta_i \frac{x_i b_p}{v^2} \left(1 - \frac{x_i b_{p,i}}{v}\right)^{\theta_i - 1} \left(1 - F_{pa,i}\right) \right) \\ \times \left(RT \left(1 - \exp\left(-\frac{N_{\text{av}} \varepsilon_{p,i}}{RT}\right)\right) - N_{\text{av}} \varepsilon_{p,i} \right), \\ b_{p,i} = \frac{N_{\text{av}}}{\rho_{\max,i}}, \\ b_p = \sum_{i=1}^{N_c} x_i b_{p,i}, \\ a_p = \sum_{i=1}^{N_c} \sum_{j=1}^{N_c} \left(x_i x_j a_{p,ij}\right), \\ a_{p,ij} = \sqrt{a_i a_j \left(1 - \frac{2}{5} \frac{\sigma_{ij}}{r_p}\right)}. \end{gathered} \tag{6}$$

In the following research, the above method has got more application and promotion. For example, Ibrahim [66] used PRC-EOS to study the phase behavior of fluids in pores of different structures with pore sizes ranging from 2 nm to 5 nm. The condensation phenomena in different pore sizes are verified, and the phase behavior in porous media is predicted. Luo et al. [67, 68] studied the mixtures' phase equilibrium after injecting methane into the Anadarko Basin shale oil. In the physical model applied in this study, the pore size distribution is discretized into specific pore sizes, which represent a multiscale system of typical pore size distribution. The simulation results show that the nanopores can reduce the fluid pressure below the bubble point, thus making the mixture subcritical. The deviation of bubble point pressure is also related to the amount of injected gas apart from pore size. The phase behavior shift in nanopores tends to contain more swelled fluid than that in the bulk state.

2.4. Interfacial Tension and Miscibility. Recent years have seen an increase in the application of CO_2 injection to enhance unconventional oil/gas recovery worldwide. This trend is due to the unique properties of CO_2, including higher solubility in crude oil, lower minimum miscible pressure, larger diffusion coefficient in nanoporous media, and higher Langmuir adsorption in shale organic matrix.

Interfacial tension (IFT) significantly affects the flow trajectory, gas-liquid equilibrium, and saturation distribution of fluids in porous media due to the cumulative contribution of Jammin effects in pores and throats to flow resistance. Also, since CO_2-brine IFT is less than that of hydrocarbon-brine, the breakthrough pressure of CO_2 may be much less than that of in situ reservoir gas [69]. Therefore, to ensure seal integrity, the CO_2 injection and storage pressure must be lower than the initial reservoir gas pressure. Moreover, the CO_2 injection pressure threshold must be predicted based on the IFT of the fluid in the specific reservoir. In other words, the IFT behavior of gas-liquid systems in unconventional reservoirs significantly affects the transport characteristics of CO_2 and the efficiency of capillary sealing. Therefore, achieving optimal CO_2 flooding and sequestration requires an accurate assessment of the IFT in the system.

Numerous experimental and simulation studies have been conducted to quantify the IFT of various gas-water systems. The most widely used IFT measurement technique is Axisymmetric Drop Shape Analysis (ADSA) method. The drops' geometric shape can be measured by the ADSA method, and then IFT can be calculated by the young-Laplace equation [70]. At present, extensive experimental measurements of IFT in gas-water systems have been made over a wide range of temperatures and pressures [70]. Chao et al. [71] explored the effective pore throat size from the perspective of the nonnegligible value of gas-water capillary force (Figure 2(a)). However, most studies have not considered the effect of nonhydrocarbon gas pollutants on system IFT, especially under high temperature/pressure conditions in reservoirs. Besides, pure water without salt is contained in most systems [72]. It has been recognized that the salinity of water does significantly affect IFT. One explanation holds that the adsorption of cations on the interface leads to the accumulation of cations in the aqueous phase. Hence, the effect of salinity on IFT is due to the interface structure changes. Another explanation is that IFT increases as the density of the aqueous increases due to the dissolved salt ions [73, 74]. Many studies listed the IFT of CO_2-water and CO_2-brine systems, and the measured temperature and pressure range were as wide as ~290-470 K and ~2-100 MPa, respectively. Factor analysis also involved the effects of salt concentration (0.085-2.75 mol/kg) and types (NaCl and $CaCl_2$) [75–78].

Besides, assessing the extent of structure and residual capture also requires a better understanding of the interfacial properties of CO_2 with in situ fluid and mineral systems. Although there is much uncertainty in the data, the CO_2 critical points measured at high pressures are very similar. Simultaneously, several similar conclusions have been found in many experimental studies: (1) in the carbon dioxide subcritical zone, IFT decreases sharply with pressure. In contrast, in the supercritical zone, IFT reaches a platform. (2) IFT usually decreases with the increase of temperature, but it reacts to more temperature dependence when CO_2 is near the critical point [79]. (3) IFT increases linearly with salt concentration [74]. Parachor Model and Scaling Law have been more widely used in IFT prediction due to their simplicity, but they cannot perform well for hydrogen-water systems. Other IFT prediction models have been reported in some studies, among which the Firoozabadi and Ramey model [80] can be used to predict IFT of oil/gas and water mixtures. Based on this, some scholars proposed a new IFT correlation by adding parameters such as compound molar mass for correction [81, 82], but their predictive ability is still limited. In the correlation of Bachu and Bennion [73], IFT is a function of salinity. This model can predict the IFT of the system based on the solubility of CO_2 in brine. However, this model is not applicable to predict IFT in the reservoir with a high temperature (>398 K) and pressure (>27 MPa). Besides, this kind of correlation can only consider the difference of temperature, pressure, and density of pure components, but it is challenging to analyze the influence of mutual solubility [78, 83].

Classical molecular dynamics (MD) has been used to predict the interfacial tension between CO_2 and water (brine) [84], as well as the CO_2-water-mineral surface contact angle [85]. The latter has been proved to be a function of temperature, pressure, and salinity. The IFT prediction accuracy depends only on whether the selected force field can reproduce the interfacial energy. However, MD simulations are limited to nanoscale studies when determining contact angles, which are smaller than most macroscopic measurements of droplet size (millimeter level). The influence of the contact line's curvature on the contact angle can be ignored in the macroscopic size of the droplet. However, at the nanoscale, the liquid and solid surface forces will change the droplet's shape, resulting in the influence of the contact line's curvature that cannot be ignored [85, 86]. The influence of contact lines is usually described by introducing contact line tension [87]. Other statistical thermodynamic methods, such as linear-gradient theory, perturbation theory, density gradient theory (DGT), integral and density

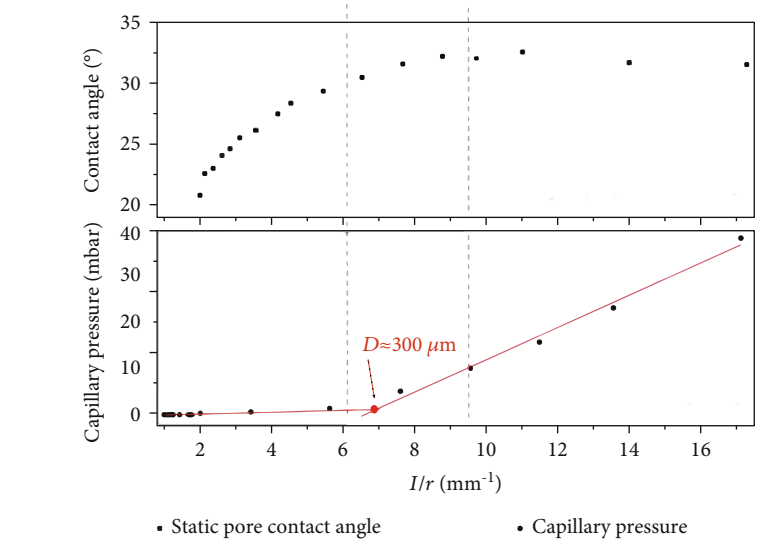

(a) Capillary pressure in inorganic mesoporous

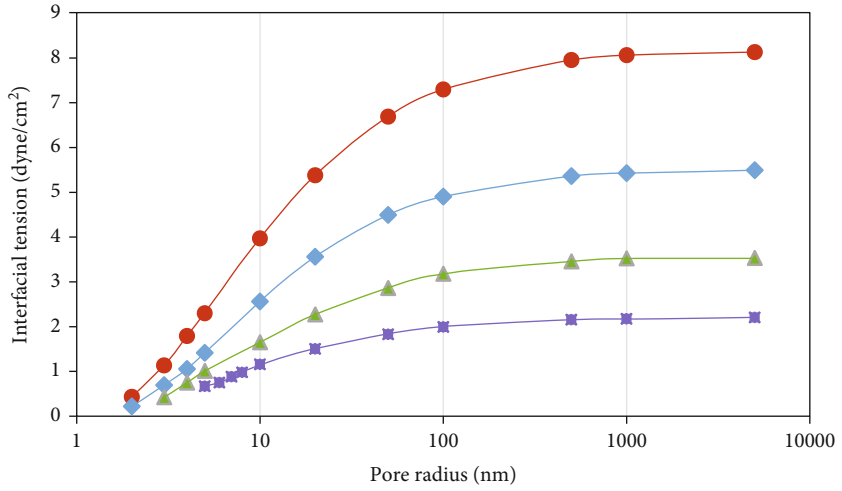

(b) IFT in organic nanopores

Figure 2: Interfacial behavior of gas-water in inorganic mesoporous (a) [71] and CO_2-oil in organic nanopores (b) [106].

functional theory (DFT), are also used to predict IFT. As a representative of the silicate strata' composition, quartz and mica have been used as the mineral base for contact angle measurement in many experiments. Some studies have also reported gas-liquid contact angles on the calcite surface (carbonate formation) [85, 88–90]. Since calcite is a suitable material to adsorb organic matters even in dilute solutions and organic materials and adsorbed ions can significantly change the wettability of mineral surfaces, the contact angle can be observed from the initial strong water wet ($0^\circ < \theta < 75^\circ$), scattering to between 2° and 60° [91]. Atomic force microscopy (AFM) data and simulations show that the adsorbed ions behave as ordered water layers on the calcite surface rather than directly binding to mineral atoms [92–94]. Also, calcite's surface properties depend mainly on the history of its exposure—CO_2 increases the acidity of water droplets, which causes calcite to dissolve, changing the local surface morphology [95].

In an oil-bearing reservoir, the injected CO_2 has two-way mass transfer with the in situ oil. CO_2 is dissolved in the oil, and hydrocarbon components in the in situ oil are extracted, and then the new mixtures are formed and further transported. As the composition of the remaining oil changes, so does the IFT of the gas-liquid system. Therefore, the initial fluid composition is considered one of the essential factors affecting IFT [96–98]. Also, there is a controversial view that the initial gas (CO_2) fraction will also have a nonnegligible influence on IFT. Earlier studies only confirmed that CO_2 fraction would affect the speed of reaching gas-liquid equilibrium [96], and later studies found that IFT also increased slightly when the initial gas-oil ratio (GOR) increased [98]. In general, IFT is positively correlated with temperature,

pressure, initial fluid composition, and feed gas to liquid ratio (FGLR). Besides, under specific temperature and pressure conditions, the system IFT after CO_2 injection can reach zero. That is, the system is entirely miscible [99]. Simultaneously, when the test pressure is higher than the mixed system's saturation pressure, zero IFT can also be observed [100]. How to distinguish clearly between miscibility and saturation needs further study.

In recent years, fluid characteristics confined in micropores and even nanopores have attracted more and more attention in practical applications. Current methods for IFT calculation and assessment of influencing factors include improved EOS equations and molecular simulations [101–105]. The general conclusion is that a decrease in pore size leads to a reduction in IFT (Figure 2(a)) [106]. The minimum miscible pressure (MMP) of CO_2 and in situ oil is an inevitable problem in the study of CO_2-EOR. As described above, apart from pore sizes, IFT is also affected by reservoir temperature, hydrocarbon composition, and initial gas-oil ratio. Therefore, these factors are also important factors affecting MMP [107]. The commonly used MMP calculation methods, including the method of characteristics (MOC), multiple mixed cells (MMC), and slim tube simulation method. However, the system MMPs in nanopores need to be calculated by combining with the modified EOS or the Perturbed-Chain Statistical Associating Fluid Theory (PC-SAFT) EOS and the Vanishing Interfacial tension (VIT) method [108]. Some calculations have found that changes in the critical properties lead to a decrease in MMP, while capillary pressure has no effect on MMP [104]. This phenomenon is mainly due to two pseudocomponents with the same critical point in the mixed system used for calculation. The IFT reaches zero after the critical point is exceeded. It has also been found that in the immiscible region (where the pressure is lower than MMP), high capillary pressure can improve the recovery efficiency of heavier components and can change MMP. However, MMP changes inconsistently with increasing capillary pressure and may decrease, increase, or remain unchanged for different mixtures. When both capillary force and critical shifts are considered, the MMP of the mixture is reduced by nanopores, but when the pore diameter is greater than 10 nm, the change of MMP can be ignored [109, 110]. In immiscible displacement, the capillary pressure effect is useful for enhancing oil recovery. However, for the miscible or near-miscible situations, the influence of capillary pressure on fluid dynamics will be compromised [111].

3. Micropore Structure Changes with CO_2 Injection

3.1. Mineral Dissolution and Deposition. Accurate prediction of petrophysical properties, the integrity of CO_2 storage seals, and flow characteristics require a full understanding of the reaction transport process [112, 113]. The reactions in this process occur between fluid-fluid (homogeneous) and fluid-solid (heterogeneous). Specifically, it can be summarized by the following two types of reactions.

$$\begin{aligned} A(aq) + B(aq) &= C(aq), \\ C(aq) + M(s) &= P(aq). \end{aligned} \tag{7}$$

Dissolved CO_2 acidifies water through the following reaction:

$$\begin{aligned} CO_2(aq) + H_2O &\leftrightharpoons H_2CO_3, \\ H_2CO_3 &\leftrightharpoons HCO_3^- + H^+, \\ HCO_3^- + H^+ &\leftrightharpoons CO_3^{2-} + H^+. \end{aligned} \tag{8}$$

The dissolution of CO_2 decreases the solution's pH and accelerates the dissolution of minerals in the host rocks. Further water-mineral reactions provide divalent cations in solution. For example, calcium-bearing plagioclase (such as anorthite) dissolution can provide Ca^{2+}. Moreover, olivine dissolution can provide Fe^{2+} and Mg^{2+}.

$$\begin{aligned} CaAl_2Si_2O_8 + 2H^+ + H_2O &\leftrightharpoons Ca^{2+} + Al_2Si_2O_5(OH)_4, \\ (Fe, Mg)_2SiO_4 + 4H^+ &\leftrightharpoons 2(Fe, Mg)^{2+} + SiO_2 + H_2O. \end{aligned} \tag{9}$$

The dissociated bicarbonate and carbonate ions could react with divalent cations in solution, precipitating as carbonate minerals:

$$\begin{aligned} (Ca, Mg, Fe)^{2+} + HCO_3^- &\leftrightharpoons (Ca, Mg, Fe)CO_3 + H^+, \\ (Ca, Mg, Fe)^{2+} + CO_3^{2-} &\leftrightharpoons (Ca, Mg, Fe)CO_3. \end{aligned} \tag{10}$$

Mineral trapping is considered the most permanent form of geologic carbon storage [114]. Mineral carbonation reactions are thermodynamically favored but proceed slowly [115]. Most minerals in sandstone reservoirs are not reactive for carbonation reactions, so it may take hundreds to thousands of years for CO_2 mineral trapping to happen [116]. Formations containing richer Ca, Mg, and Fe can potentially result in mineral trapping over much shorter time scales.

In the case of an evolving porous medium affected by mineral dissolution-precipitation reactions, it is evident that both porosity and connectivity can be affected. The dissolution of a solid phase is directly linked to the increase of the overall porosity. However, dissolution does not necessarily increase effective porosity to the same degree. The effect can be substantial if dissolution widens and opens up pore throats or opens up new diffusion pathways [117, 118]. It can be more limited if dissolution is more equally distributed [119]. Similarly, mineral precipitation might have a limited effect on connectivity if minerals form on existing surfaces without clogging pore throats.

On the other hand, precipitation may lead to the disconnection of existing solute migration pathways [119], with a pronounced impact on flow and transport parameters [120–122]. These theoretical considerations imply the dissolution, and precipitation of minerals can lead to very different impacts on effective porosity and connectivity with the same total porosity change. The porous media's total porosity includes transport pores φ_{tra}, dead-end pores, and isolated

pores. Apart from the isolated pores where the fluids cannot directly contact injected gas, mass transfer between CO_2 and in situ fluids occurs in the open pores φ_{open} (including transport pores and dead-end pores). The dissolution/precipitation caused by chemical reactions may penetrate or increase some of the isolated pores and change the critical radius r_{cr} and tortuosity τ that affecting bubbles to pass through. Therefore, the total porosity, effective porosity, and pore-throat connectivity have a combined effect on tortuosity and permeability, affecting flow and migration (Figure 3) [123, 124]. After the acid fluid comes into contact with the mineral, the dissolution occurs in the undersaturated state, increasing fracture aperture. Mineral precipitation may occur when the concentration of necessary hydrates reaches a certain threshold after mineral dissolution [125–127]. For example, gypsum may precipitate after calcite is dissolved [128, 129], and calcite may precipitate after dolomite is dissolved. In these cases, fracture permeability change direction and extent depend on the interplay between dissolution and precipitation.

In the early stage, some short-term reaction experiments related to CO_2 injection were proposed. Rock samples with different permeabilities were prepared by hot pressing of calcite powder and quartz powder, and then CO_2 was injected into the samples. Based on micro-CT imaging, pore microstructure changes during limestone dissolution can be observed, and the power-law relationship between permeability and porosity can be proposed [130, 131]. However, in the macroscopic reservoir, the solute is not evenly distributed in the heterogeneous porous medium. This feature may lead to a deviation in the estimation of the reaction rate [132]. By comparing the Poiseuille flow model with a well-mixed reactor model, Li et al. [133] studied the rate of mineral reactions in a single pore and fracture and discussed the physical model scale's impact. In short-term experiments on Tensleep sandstone and Berea sandstone (mainly dolomite and anhydrite cement), core samples were washed by CO_2 for several days after saturated salt solution. It was found that the precipitation of minerals led to a decrease in permeability despite the presence of mineral dissolution [134, 135]. Another experiment on sandstone samples cemented with calcite and dolomite showed that the dissolution of carbonate minerals led to an increase in permeability [136]. This increase is due to enhanced pore modification and is related to the dissolution of carbonate cement bonds. In the long run, minerals in the formation that react with CO_2 in brine include calcite, siderite, dolomite, quartz, barite, muscovite, feldspar, and clay minerals [137, 138]. Chemical reactions will dissolve minerals, weaken cementation, weaken particle time bonding, and alter flow characteristics, thereby affecting CO_2 displacement and storage operations' efficiency and safety.

Given the complexity and heterogeneity of pore structures, extensive chemical disturbances, and the coupling between these different processes, it is difficult to obtain quantitative assessments of dissolution patterns and rates and feedback on porosity and permeability based solely on theoretical considerations. Recent advancements in imaging techniques, such as X-ray microtomography [139] and

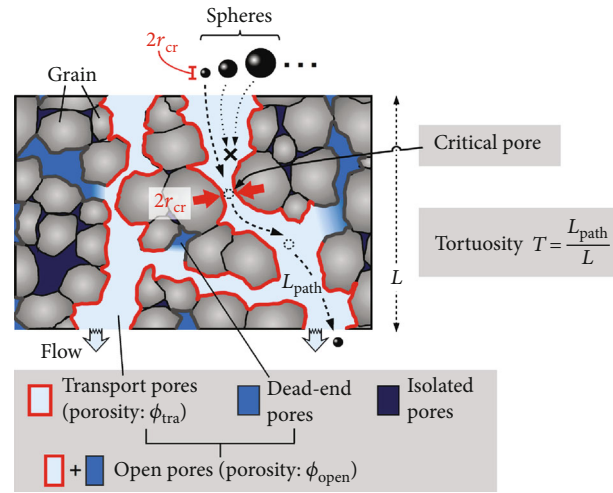

Figure 3: Schematic diagram of pore structure. Definitions of total porosity and effective porosity [124].

nuclear magnetic resonance (NMR) [140], allow visualization of pore structures at submicron resolutions, providing a window into the complex properties of porous media. Simultaneously, various methods ranging from traditional computational fluid dynamics techniques to smooth particle hydrodynamics and lattice Boltzmann methods have been proposed to simulate the flow of porous media [141–144]. With improved imaging technology combined with the development of pore-scale model formulations [123, 145, 146] and substantial advances in computational power, the exploration of processes on the pore scale has become possible from both an experimental and modeling perspective [147–150].

The pore network model comprises interconnected throats and pores, reflecting the complex structure of porous media. Many scholars use the pore network model to characterize the physical and mineral properties of porous media. Li et al. [151] and Raoof et al. [152] studied the chemical reaction rate in porous media by using the pore network model and established the relationship between the Peclet number and the adhesion/separation coefficient of adsorbents. The pore network model has also been used to study chemical reactions on porosity, permeability, and the correlation between them in the homogeneous system [119]. Tansey et al. [153] proposed a mass transfer coefficient correlation and pore-merging criterion by simulating carbonate rocks' dissolution. The pore-scale model and the direct simulation based on finite-difference were used to solve the Stokes equation and convection-diffusion equation. However, the comparison of the results showed that the pore network model was better adapted to the case of larger velocity and reaction rate under the same situation [154]. Besides, the pore network model also has some limitations. For example, it is difficult or sometimes impossible to extract representative pore network models for heterogeneous porous media [155].

A Lattice Boltzmann method (LBM) was developed to simulate the porosity scale dissolution and precipitation [156]. The method can simulate the multicomponent reaction transport process under different temperatures and

pressures. Also, LBM can be developed to simulate reactive multiphase flows in arbitrary geometric pores. The temporal and spatial distribution of each constituent phase and the reactants' evolution during the dissolution/precipitation process are reflected [157]. As mentioned earlier, the nonuniform distribution of reactants in the heterogeneous pore structure will result in differences in the local reaction rate.

On the one hand, the researchers established a pore-scale numerical model based on LBM. On the other hand, a continuous scale numerical model directly simulated is also established. By comparing the results of the two simulations, it was found that the inhomogeneity of the flow field would reduce the reactivity of the system. The more substantial the pore structure's heterogeneity was, the more pronounced the reduction was, leading to the difference in the velocity of the reaction front between different models [112, 158]. Combining the LBM method with the flow-solid interface tracking method can predict the positive and negative effects of mineral dissolution/precipitation on porous media [159] and the relationship between permeability and porosity [160]. The numerical results' complexity is reflected in the fact that the correlation between pore and permeability is highly dependent on Peclet and Damkohler systems and the porous medium structure. Extending the LBM method, the effects of decomposition, dissolution, and precipitation in fluid-mineral systems on multiphase transport can be discussed in depth [161].

3.2. Asphaltene Precipitation. The precipitation and deposition of long-chain alkanes (mainly asphaltenes) in conventional reservoirs' pore space have been studied extensively. Researchers define phase precipitation as a solid phase transformed by a liquid phase, whereas deposition refers to a precipitate (solid phase) attachment to a rock surface (Figure 4) [162]. The current asphaltene precipitation thermodynamic models assume including colloid-based methods and solubility-based methods. The model based on the colloidal approach assumes that asphaltenes are suspended solid particles, which are colloidal in the system. Physical and chemical reactions disrupt the thermodynamic equilibrium, which may cause the outer layer rupture and asphaltene flocculation [163]. The method assumes that the asphaltene components based on solubility can be decomposed into the components and settling components, the precipitation components can dissolve in the oil and form a solution, and precipitation occurred in solid-liquid equilibrium (SLE) or liquid-liquid equilibrium (LLE) state, can through the SLE solubility model and another physical model to forecast the asphaltene flocculation [164]. There are three types of asphaltene precipitation theoretical studies: using the Support Vector Machine (SVM) model to study the development of asphaltene precipitation [165]; applying the Computational Fluid Dynamics Method to investigate the molecular deposition of asphaltic materials [166, 167]; and using molecular simulations to understand asphaltene deposition behavior by studying interactions between different components of molecules [168].

In the process of gas injection for oil recovery, the injected gases change the inherent dispersion system of colloids and asphaltenes in crude oil, leading to instability of asphaltenes, which in turn leads to viscous solid deposition [169]. On the one hand, asphaltenes are adsorbed on reservoir rocks, blocking pore throats or changing formation wettability, reducing hydrocarbon fluids' mobility [170]. On the other hand, asphaltene deposition can cause severe formation damage to reservoirs, especially near production wells with the most remarkable pressure drop. Asphaltenes can also flocculate on rock surfaces. Flocs rupture during dissociation and plug the pore openings of the reservoir [162]. Different injection gases have different effects on asphaltene precipitation. The injection of CH_4, CO_2, and N_2 will lead to asphaltene precipitation, among which N_2 has the most significant influence on asphaltene precipitation [171, 172], followed by CH_4 [173].

According to the currently known, there are three main reasons for the asphaltenes caused by CO_2 injection. The first one is the changes in temperature and pressure [174, 175]. Studies have confirmed that the temperature drop caused by CO_2 injection in the near-well zone would result in asphaltene precipitation [174]. The size of asphaltene aggregates in CO_2 is negatively correlated with temperature, and the nonmonotonic effect of pressure on aggregates can also be observed. Asphaltene deposition reaches its peak value at the oil bubble point [176]. Also, resins or other polymers' presence limits the tendency of asphaltenes to accumulate in CO_2 [177–179]. When the fluid pressure exceeds MMP, asphaltenes begin to precipitation. When the system pressure is below the MMP, the pore blockage damage is much less than when the pressure is higher than MMP. This is because the resins that stabilize asphaltenes are more unstable when pressure is higher than MMP [180–183]. The second reason is CO_2 concentration [184]. Some other studies have shown that the flocculation of asphalts in single-phase mixtures of petroleum and carbon dioxide has nothing to do with pressure but only with carbon dioxide concentration. They also found that asphaltene flocculation increased linearly with the increase of CO_2 concentration [185]. Compared with heptane and toluene, asphaltene stable aggregates in supercritical carbon dioxide have a longer lifetime [186]. Wang and Ferguson [187] used the force field to establish a mesoscale method for studying asphaltene aggregation. A flexible structure is used to deal with carbon dioxide. Visual molecular dynamics (VMD) was used to prepare visualizations [188]. Mehana et al. studied the system's physical conditions and composition on asphaltene aggregation dynamics [189]. The third reason is separation and selective extraction by CO_2 [190]. When the lighter components are extracted and carried away by CO_2, the remaining hydrocarbon mixtures' molecular weight gradually increases, increasing the risk of asphaltene precipitation and formation damage. What is more, asphaltene precipitation is closely related to the composition of rocks and minerals. Calcite content is positively correlated with asphaltene deposition [175], while iron content is negatively correlated with asphaltene deposition [191]. Most asphaltene crude oils have increased wettability on mica surface [192]. Due to the higher wettability of reservoir crude oil, the content of bound water in pores decreases (from 26.5% to 10.7%), leading to increased water

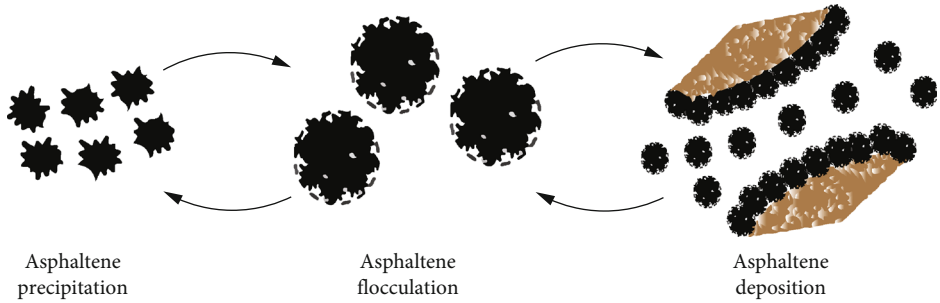

Figure 4: Schematic diagram of asphaltene evaluation in porous media.

production and decreased final oil recovery [193]. The presence of water will lead to a reduction of asphaltene precipitation [194]. This reduction is due to the buffering properties of the formation brine.

At present, there are little researches on how asphaltenes in crude oil behave in micropores and nanopores during CO_2 injection. Mohammad et al. [195] simulated asphaltene deposition and studied the optimal CO_2 injection during saline-CO_2 cycle displacement to improve the recovery of low permeability reservoirs by CO_2 flooding. Shen and Sheng [196] studied asphaltene deposition produced by cyclic CO_2 injection into the Eagle Ford Shale. However, this study was conducted at room temperature (~25°C) and 0.3 MPa pressure, and no mechanism of asphaltene precipitation, deposition, and plugging in nanoporous has been reported. Fakher and Imqam [197] found that because unconventional reservoirs' pore size is close to the size of asphaltene clusters, the asphaltene is difficult to extrude from pores. A large amount of asphaltene accumulates in the nanopore and blocks the rock matrix severely. Sun et al. [198] studied the competitive adsorption of asphaltenes by carbon dioxide and nitrogen in nanopores to study the feasibility of using asphaltenes as a means of carbon capture in nanopores during carbon dioxide injection.

3.3. Stress Field Redistribution. Although CO_2 has long been injected into depleting reservoirs to enhance oil and gas recovery, there is a relatively little field experience in conducting geological CO_2 storage in oil layers than the mature and commercially viable technology of pumping CO_2 underground. A significant difference between CO_2-EOR and CCS is the cost of CO_2 as a displacing agent. EOR is intended to make a profit by reducing the injection of CO_2 and reuse it after being produced as a dissolved gas. However, the goal of CCS is to maximize the storage of CO_2 and permanently trap it in place. In the past few decades, the scientific literature has discussed issues related to the sequestration of CO_2 underground from the perspectives of hydrodynamics, geochemistry, and geomechanics [199–204].

Pore pressure buildup induced by CO_2 injection depends on formation capacity, transport properties, and aquifer connectivity [205, 206]. Formation transport and geomechanical properties, including porosity, permeability, and pore compressibility, determine CO_2 plume movement and local pore pressure changes. These formation properties vary considerably with rock types and spatial heterogeneity, significantly impacting CO_2 trapping and migration. Pressure changes induced by CO_2 injection operations alter stress at the geological carbon storage (GCS) site. For example, changes in geomechanical conditions may result in mechanical failure of the reservoir or reservoir expansion. Stress arching may increase the vertical stress over the reservoir and lead to normal fault activation. Intricate stress transfer patterns between reservoir and caprock, associated with the lithologies' poroelastic properties and the reservoir stress path resulting from the injection, could result in tensile or shear failures and enhanced fluid flow. These reservoir mechanics changes caused by stress field redistribution may also provide pathways for CO_2 leakage or trigger induced seismicity. Maintaining CO_2 injection for several years will lead to a large pressurization area within the reservoir [207]. Even if the CO_2 diffusion radius is only a few kilometers, the pressure perturbation cone's radius with overpressure higher than 0.1 MPa can exceed several hundred kilometers [208]. Because of the similarities between CO_2 injection and other subsurface activities involving fluid injection, the seismic risk associated with carbon storage operations is real, and risk assessment is critical to informing any decision-making from site characterization to the determination of operational parameters.

Some researches suggested that the high pore pressure could cause hydraulic fractures in the shale caprock [209, 210]. The fractures or cracks generate the structural environment (including squeeze, stretch or slip), stress difference, and the amount and orientation of brittle ruptures [211]. These stress characteristics describe the leak-off of oil and gas through expanding fractures developed in overpressure reservoirs. In this case, the fractures can reseal when the formation returns to its normal state of pressure [210]. To prevent the formation of these cracks or fissures, the researchers propose limiting the injection pressure below the minimum stress (the minimum pressure that causes tensile fractures).

However, some studies [211] suggest that tensile cracking can occur only under relatively low-stress differential conditions. In their view, the stress caused by reservoir expansion in the caprock is not the cause of the fault generation, despite the possibility of shear failure at the reservoir-cap interface and hydraulic fractures extending from the reservoir to the caprock above. At the same time, they emphasize that reactivation of existing faults is a greater risk, or even one of the significant risks, of triggering cap leakage (Figure 5) [212]. Changes in the in situ stress conditions associated with

subsurface activities can cause suitably oriented faults or fractures to slip because of shear. Fractures that are oriented to maximize the possibility of slip are referred to as "critically oriented" fractures.

Similarly, fractures that would require only a minor increase in fluid pressure to slip are referred to as "critically stressed" fractures. Higher pressure cutoffs that may induce fault stability issues in critically stressed faults, such as 1 MPa, can extend tens of kilometers [208, 213]. Furthermore, once large-scale geologic carbon storage projects are fully deployed, the superposition of overpressure from different injection wells in the same sedimentary basin is expectable, leading to an even larger pressurized region [214]. Thus, even though injection wells will most likely be placed far away from identified faults to minimize the risk of fault reactivation, overpressure will eventually reach faults in the far field, affecting their stability [215]. For any activities involving fluid injection, evaluating critically stressed fractures is fundamental for understanding the placement and orientation of injecting wells, determining the main operational parameters such as the injection rate and maximum allowable injection pressure allowed, or deploying a risk-based monitoring strategy.

On the other hand, the variations in pore structures due to reaction have a significant impact not only on petrophysical properties but also on the porous media's mechanical properties. In reactive transport, porosity changes due to reaction. This results in significant variations in the porous media's mechanical properties [216].

Stress and strain changes depend on the number of reactants and the amount of dissolution and precipitation produced in the pore structure. Specifically, due to the lack of active minerals, only minor chemical-mechanical changes are expected in most quartz-sandstone and unconsolidated sandstone when exposed to CO_2. In terms of geomechanical property types, sandstone with "CO_2-weak" intergranular cement is the most easily changed rock. Even a small amount of reaction can significantly impact the geomechanical properties that depend on cementation. For some types of rock, including carbonate-cemented sandstones (e.g., Entrada sandstone and Castlegate sandstone) and clay-cemented sandstones (Chlorite-cemented Tuscaloosa sandstone and Mt. Simon sandstone) [217], dissolution and degradation of the pressure consolidation will result in (1) decreases of cohesive strength, fracture toughness, and yield stress locus size; (2) increases of compliance and creep; (3) changes in post-peak behavior; and (4) changes in frictional behavior [217–221]. When granular-supported carbonate rocks (e.g., chalk) are exposed to acidified (dissolved CO_2) brines, significant stresses occur [222]. Pores in carbonate rocks will expand significantly, but the rocks' mechanical properties will not change much until a large number of rock minerals are dissolved [223]. In carbonate-rich shale, soluble minerals are distributed in sheets between soluble bedrock and cement sandstone [224]. However, due to the difficulties in sample processing and pore structure protection, core-scale CO_2 and shale cap reaction experiments are limited [225].

Chemical-stress interactions in the reservoir can lead to wellbore stability issues [113] and CO_2 storage safety risks. First, chemical reactions that dissolve minerals can cause rock damage, increasing the risk of wellbore collapse. Simultaneously, the reaction of CO_2 with minerals reduces the mechanical strength of the formation containing brine, which may lead to CO_2 leakage [226]. Therefore, it is crucial to understand the influence of reaction flow on mechanical rock properties in CCUS. Madland et al. [227] studied the mechanical stability of chalk after saturated by CO_2 gas and carbonic acid water. The results show that the influence of CO_2 gas on the strength of chalk is small, while that of carbonated water is great. Farquhar et al. [228] tested the mineral and porosity changes of sandstone and siltstone after reacting with low-salinity water and supercritical carbon dioxide (SC-CO_2). The test results showed that the calcite content decreased from 17 vol % to 15 vol % after the reaction, and the porosity increased by 1.1 vol %. CO_2-water-rock interaction also causes cap deformation, leading to significant stress and stress-induced permeability changes [229, 230]. Few studies have focused on the effect of the reaction on porous media's mechanical properties, and the design of CO_2 injection schemes for unconventional reservoirs often ignores the strain and stress caused by chemistry.

4. Challenges and Suggestions

Unconventional reservoirs are characterized by organic and inorganic matters, diverse mineral compositions, nonignorable capillary forces, and phase state changes under micro-nanopores' confinement [231]. The surface wettability and adsorption characteristics of different minerals present great complexity. Therefore, incorporating the processes that occur inside mineral nanopores and recognize the flow characteristics of CO_2 in the matrix and natural-hydraulic fracture system is extremely difficult.

Due to the dense matrix rock, injected CO_2 first passes quickly through the fracture. Then, affected by the pressure gradient, CO_2 seeps into the matrix and replaces the in situ oil in it. As more crude oil enters the fracture and the bulk CO_2, the injected CO_2 permeates into the matrix. After that, the oil in the bulk CO_2 is driven out due to the expansion and viscosity decrease. Finally, the dominating driving force changes to concentration gradient diffusion from matrix to fracture with the continuing decline pressure gradient. In the current studies, the nanopore confinement affects the molecular density distribution and phase behavior, which results in the difference of gas-liquid equilibrium, interfacial tension, capillary force, and miscibility from that in conventional millimeter porous media [232]. Simultaneously, mineral dissolution and precipitation, asphaltene precipitation, and stress field changes caused by chemical/physical reactions between fluids and rocks may change the geometric characteristics and connectivity of pores, affecting the apparent permeability of fluids.

On the other hand, after CO_2 is injected into the pores of shale containing water or oil, the rock surface's wettability will significantly change, further affecting the microscopic migration mechanism of fluid components in the reservoir. The film formed by CO_2 adsorption can transform the local hydrophilic surface in kerogen pores into a superhydrophobic

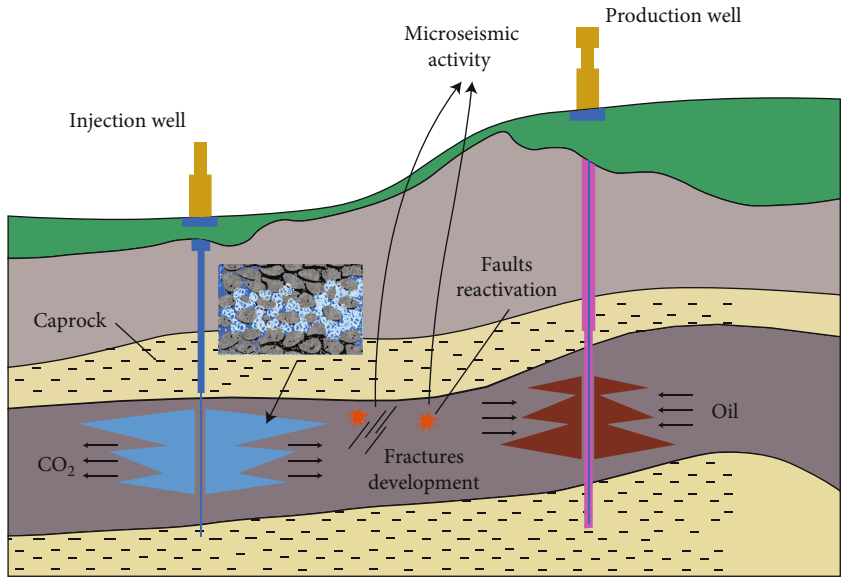

Figure 5: Stress activities with CO_2 injection.

surface on the surface of organic matter, reducing the flow resistance of formation water [233]. On the surface of inorganic matter, CO_2 can peel off the nonpolar components of in situ oil, leaving the polar components, and enhance the hydrophilicity by selective extraction [234]. In the formation of water, CO_2, and pore surface, CO_2 can make mica and quartz surfaces with strong water wettability behave as neutral wetting. This phenomenon is significantly affected by mineral concentration [235]. Although it is not apparent, the boundary slip exists in the oil phase displaced by CO_2 in the inorganic pores. The flow of formation water will change from nonslip boundary to slip boundary on the kerogen pore surface after forming an absorption layer of CO_2 [236]. The change of wettability leads to more complicated diffusion and migration rules of multiphase fluid confined to the nanopore.

Fluid migration in the subsurface can induce changes in phase state, mechanical stresses, and the fluid and natural geological material chemistry. In many situations, changes in all processes give a coupled response, in that one process feeds back to another. When trying to understand CO_2-oil flow through nanoscale porous media, it is essential to identify the relative importance of the processes occurring and the degree of interactions. Modeling of such highly nonlinear coupled flow should be involved, but current and predicted computational ability could not simulate all the known and physically described processes operating efficiently [237–239]. Although CO_2 injection has been widely used in conventional reservoirs to enhance oil and gas recovery, the interaction of CO_2 with fluids and pore surface in unconventional formations will influence phase behavior and multiphase flow, thus affecting CO_2 capture and reservoir stress redistribution. However, the current research results cannot reasonably explain and describe these changes. Most large-scale simulations of CO_2 storage intrinsically neglect the complex and vital interaction between CO_2 and multicomponent mobile liquid hydrocarbons.

5. Conclusions

This review summarizes some fluid-fluid and fluid-solid systems' physical and chemical reactions with CO_2 injection into unconventional reservoirs. Also, the resultant change of pore structure and connectivity is discussed in this paper. Regarding the limitation recently, the challenges and some suggestions of CCUS for the future are proposed. Based on this review, the following conclusions are drawn below.

(1) It is a practical experimental method to study the phase behavior through microfluidic technology. Moreover, the visualization method of nanofluids can observe some unique phenomena of nanoscale phase transition. Theoretical approaches like MD and DFT can make up for high-cost defects and are limited to high temperature and pressure conditions in the microscopic phase experiment

(2) The modified EOS can be used to deal with VLE calculation, including nanopore confinement effect, but further investigation is needed to predict the phase behavior for long-chain hydrocarbon mixture within a wide temperature and pressure range

(3) Molecular simulation technology has been widely used to study the adsorption/desorption of CO_2 in micro-nanoscale pores. In recent years, we see the crescent studies of microscopic interaction between CO_2 and heavier oil components

(4) Salinity and temperature affect interface properties of CO_2-brine-mineral system. The specific phase behavior will change the IFT and alter the MMP in oil-bearing nanopores

(5) In addition to total porosity, mineral dissolution and precipitation of minerals may have a very different impact on effective porosity and connectivity.

Improved imaging techniques, combined with numerical methods, provide a solution for long-term pore geometry changes and permeability feedback

(6) CO_2 extraction may increase the risk of asphaltene deposition, which may block pore throats or alter formation wettability. However, more researches are needed for the performance of asphaltenes in microns and nanopores after CO_2 injection

(7) The mechanical properties of rocks are affected by CO_2 pressurization and the chemical reaction. The resulting stress changes can cause rock damage or pose a microseismic risk to the formation, opening microfractures, restarting faults, or creating artificial fractures

(8) The study of CCUS operation and safety assessment in unconventional reservoirs requires the coupling of phase behavior, fluid and geological change, and stress field redistribution

Nomenclature

a_p: van der Waals energy parameter modified by confinement
b_p: van der Waals volume parameter modified by confinement
d_p: Pore diameter
F_p: The fraction of the fluid molecules in the confined space
f: Fugacity
g_s: Granular size
N_{av}: Avogadro's number
N_c: Index denotes the number of fluid components of the mixture
P: Pressure
P_b: Bubble point pressure
P_{cap}: Capillary pressure
P_d: Dew point pressure
r_p: Pore radius
T: Absolute temperature
v: Molar volume of the fluid
x: Liquid molar fraction
y: Vapor molar fraction.

Greek letters

α: Contact angle
δ: Interfacial tension
ε: Lennard-Jones energy parameter
ε_p: Molecule-wall interaction energy parameter
θ: Geometric term
ρ_{max}: Confinement-modified molecular packing density
σ_{ij}: Average molecular diameter for components i and j
σ_{LJ}: Lennard-Jones size parameter
ϕ: Fugacity coefficient.

Subscripts

a: Adsorbed phase
b: Bulk phase
i, j: Component index notations
c: Critical properties
cp: Pore critical properties
L: Liquid phase
V: Vapor phase.

Data Availability

All the data is presented in the manuscript.

Conflicts of Interest

The authors declare that they have no known competing financial interests or personal relationships that could have appeared to influence the work reported in this paper.

Acknowledgments

This project was supported by the National Natural Science Foundation of China (No. 51974348) and the Graduate Innovative Engineering Project of China University of Petroleum (No. YCX2018017).

References

[1] A. Muggeridge, A. Cockin, K. Webb et al., "Recovery rates, enhanced oil recovery and technological limits," *Philosophical Transactions of the Royal Society A: Mathematical, Physical and Engineering Sciences*, vol. 372, no. 2006, article 20120320, 2014.

[2] A. O. Gbadamosi, R. Junin, M. A. Manan, A. Agi, and A. S. Yusuff, "An overview of chemical enhanced oil recovery: recent advances and prospects," *International Nano Letters*, vol. 9, no. 3, pp. 171–202, 2019.

[3] H. Jia and J. J. Sheng, "Discussion of the feasibility of air injection for enhanced oil recovery in shale oil reservoirs," *Petroleum*, vol. 3, no. 2, pp. 249–257, 2017.

[4] H. Belhaj, H. Abukhalifeh, and K. Javid, "Miscible oil recovery utilizing N_2 and/or HC gases in CO_2 injection," *Journal of Petroleum Science and Engineering*, vol. 111, pp. 144–152, 2013.

[5] Global CCS Institute, *Capacity of Operational Large-Scale Carbon Capture and Storage Facilities Worldwide as of 2019*, The Global Status of CCS Report, 2020.

[6] A. Y. Ku, P. J. Cook, P. Hao et al., "Cross-regional drivers for CCUS deployment," *Clean Energy*, vol. 4, no. 3, pp. 202–232, 2020.

[7] I. Langmuir, "The adsorption of gases on plane surfaces of glass, mica and platinum," *Journal of the American Chemical society*, vol. 40, no. 9, pp. 1361–1403, 1918.

[8] R. I. Masel, *Principles of Adsorption and Reaction on Solid Surfaces*, John Wiley & Sons, 1996.

[9] S. Zhan, Y. Su, Z. Jin, W. Wang, and L. Li, "Effect of water film on oil flow in quartz nanopores from molecular perspectives," *Fuel*, vol. 262, article 116560, 2020.

[10] S. Molla and F. Mostowfi, "Microfluidic platform for PVT measurements," in *SPE Annual Technical Conference and Exhibition*, Amsterdam, The Netherlands, October 2014.

[11] N. Y. Rapoport, A. M. Kennedy, J. E. Shea, C. L. Scaife, and K. H. Nam, "Controlled and targeted tumor chemotherapy

by ultrasound-activated nanoemulsions/microbubbles," *Journal of Controlled Release*, vol. 138, no. 3, pp. 268–276, 2009.

[12] N. Karadimitriou, S. Hassanizadeh, V. Joekar-Niasar, and P. J. Kleingeld, "Micromodel study of two-phase flow under transient conditions: quantifying effects of specific interfacial area," *Water Resources Research*, vol. 50, no. 10, pp. 8125–8140, 2014.

[13] P. Chareonsuppanimit, S. A. Mohammad, R. L. Robinson Jr., and K. A. M. Gasem, "High-pressure adsorption of gases on shales: measurements and modeling," *International Journal of Coal Geology*, vol. 95, pp. 34–46, 2012.

[14] T. Zhang, G. S. Ellis, S. C. Ruppel, K. Milliken, and R. Yang, "Effect of organic-matter type and thermal maturity on methane adsorption in shale-gas systems," *Organic Geochemistry*, vol. 47, pp. 120–131, 2012.

[15] M. Bergaoui, A. Nakhli, S. al-Muhtaseb, and M. Khalfaoui, "Adsorption process of *n* -alkanes onto BAX-1100 activated carbon: theoretical estimation of isosteric heat of adsorption and energy distribution of heterogeneous surfaces," *Journal of Molecular Liquids*, vol. 252, pp. 399–407, 2018.

[16] R. J. Ambrose, R. C. Hartman, M. Diaz-Campos, I. Y. Akkutlu, and C. H. Sondergeld, "Shale gas-in-place calculations part I: new pore-scale considerations," *Spe Journal*, vol. 17, no. 1, pp. 219–229, 2011.

[17] B. R. Didar and I. Y. Akkutlu, "Pore-size dependence of fluid phase behavior and properties in organic-rich shale reservoirs," in *SPE International Symposium on Oilfield Chemistry*, The Woodlands, Texas, USA, April 2013.

[18] K. Mosher, J. He, Y. Liu, E. Rupp, and J. Wilcox, "Molecular simulation of methane adsorption in micro- and mesoporous carbons with applications to coal and gas shale systems," *International Journal of Coal Geology*, vol. 109-110, pp. 36–44, 2013.

[19] K. Zeng, P. Jiang, Z. Lun, and R. Xu, "Molecular simulation of carbon dioxide and methane adsorption in shale organic nanopores," *Energy & Fuels*, vol. 33, no. 3, pp. 1785–1796, 2019.

[20] Y. Liu, X. Ma, H. A. Li, and J. Hou, "Competitive adsorption behavior of hydrocarbon(s)/CO_2 mixtures in a double-nanopore system using molecular simulations," *Fuel*, vol. 252, pp. 612–621, 2019.

[21] M. S. Santos, L. F. Franco, M. Castier, and I. G. Economou, "Molecular dynamics simulation ofn-alkanes and CO2confined by calcite nanopores," *Energy & Fuels*, vol. 32, no. 2, pp. 1934–1941, 2018.

[22] R. Tindy and M. Raynal, "Are test-cell saturation pressures accurate enough," *Oil and Gas Journal*, vol. 64, no. 49, pp. 126–139, 1966.

[23] F. Trebin and G. Zadora, "Experimental study of the effect of a porous medium on phase changes in gas-condensate systems," *Izv Vyssh Uchebn Zaved, Neft Gaz;(USSR)*, vol. 8, 1968.

[24] P. Sigmund, P. Dranchuk, N. Morrow, and R. A. Purvis, "Retrograde condensation in porous media," *Society of Petroleum Engineers Journal*, vol. 13, no. 2, pp. 93–104, 1973.

[25] M. Thommes and G. H. Findenegg, "Pore condensation and critical-point shift of a fluid in controlled-pore glass," *Langmuir*, vol. 10, no. 11, pp. 4270–4277, 1994.

[26] G. Findenegg, S. GroB, and T. Michalski, "Pore condensation in controlled-pore glass. An experimental test of the Saam-Cole theory," *Studies in Surface Science and Catalysis*, vol. 87, pp. 71–80, 1994.

[27] V. P. Voronov, M. Y. Belyakov, E. E. Gorodetskii, V. D. Kulikov, A. R. Muratov, and V. B. Nagaev, "Phase behavior of methane-pentane mixture in bulk and in porous media," *Transport in Porous Media*, vol. 52, no. 2, pp. 123–140, 2003.

[28] S. Qiao, S. Bhatia, and X. Zhao, "Prediction of multilayer adsorption and capillary condensation phenomena in cylindrical mesopores," *Microporous and mesoporous materials*, vol. 65, no. 2-3, pp. 287–298, 2003.

[29] H. Vinh-Thang, Q. Huang, M. Eić, D. Trong-On, and S. Kaliaguine, "Adsorption of C7 hydrocarbons on biporous SBA-15 mesoporous silica," *Langmuir*, vol. 21, no. 11, pp. 5094–5101, 2005.

[30] P. Zeigermann, M. Dvoyashkin, R. Valiullin, and J. Kärger, "Assessing the pore critical point of the confined fluid by diffusion measurement," *Diffusion Fundamentals*, vol. 11, no. 41, pp. 1-2, 2009.

[31] P. Russo, M. M. L. Ribeiro Carrott, and P. Carrott, "Trends in the condensation/evaporation and adsorption enthalpies of volatile organic compounds on mesoporous silica materials," *Microporous and Mesoporous Materials*, vol. 151, pp. 223–230, 2012.

[32] S. Luo, J. L. Lutkenhaus, and H. Nasrabadi, "Experimental study of confinement effect on hydrocarbon phase behavior in nano-scale porous media using differential scanning calorimetry," in *SPE Annual Technical Conference and Exhibition*, Houston, Texas, USA, September 2015.

[33] E. Barsotti, S. P. Tan, M. Piri, and J. H. Chen, "Phenomenological study of confined criticality: Insights from the capillary condensation of propane, n-butane, and n-pentane in nanopores," *Langmuir*, vol. 34, no. 15, pp. 4473–4483, 2018.

[34] S. P. Tan, E. Barsotti, and M. Piri, "Application of material balance for the phase transition of fluid mixtures confined in nanopores," *Fluid Phase Equilibria*, vol. 496, pp. 31–41, 2019.

[35] X. Qiu, S. P. Tan, M. Dejam, and H. Adidharma, "Isochoric measurement of the evaporation point of pure fluids in bulk and nanoporous media using differential scanning calorimetry," *Physical Chemistry Chemical Physics*, vol. 22, no. 13, pp. 7048–7057, 2020.

[36] B. Coasne, K. E. Gubbins, and R. J.-M. Pellenq, "Temperature effect on adsorption/desorption isotherms for a simple fluid confined within various nanopores," *Adsorption*, vol. 11, no. S1, pp. 289–294, 2005.

[37] R. R. Kotdawala, N. Kazantzis, and R. W. Thompson, "An application of mean-field perturbation theory for the adsorption of polar molecules in nanoslit-pores," *Journal of mathematical chemistry*, vol. 38, no. 3, pp. 325–344, 2005.

[38] A. V. Neimark, P. I. Ravikovitch, and A. Vishnyakov, "Inside the hysteresis loop: multiplicity of internal states in confined fluids," *Physical Review E*, vol. 65, no. 3, article 031505, 2002.

[39] N. Sobecki, C. Nieto-Draghi, A. di Lella, and D. Y. Ding, "Phase behavior of hydrocarbons in nano-pores," *Fluid Phase Equilibria*, vol. 497, pp. 104–121, 2019.

[40] J. D. Van der Waals, *Over de Continuiteit van den Gas-en Vloeistoftoestand*, Sijthoff, 1873.

[41] O. Redlich and J. N. Kwong, "On the thermodynamics of solutions. V. An equation of state. Fugacities of gaseous solutions," *Chemical Reviews*, vol. 44, no. 1, pp. 233–244, 1949.

[42] D. Zudkevitch and J. Joffe, "Correlation and prediction of vapor-liquid equilibria with the redlich-kwong equation of state," *AIChE Journal*, vol. 16, no. 1, pp. 112–119, 1970.

[43] G. Soave, "Equilibrium constants from a modified Redlich-Kwong equation of state," *Chemical Engineering Science*, vol. 27, no. 6, pp. 1197–1203, 1972.

[44] D.-Y. Peng and D. B. Robinson, "A new two-constant equation of state," *Industrial & Engineering Chemistry Fundamentals*, vol. 15, no. 1, pp. 59–64, 1976.

[45] G. Schmidt and H. Wenzel, "A modified van der Waals type equation of state," *Chemical Engineering Science*, vol. 35, no. 7, pp. 1503–1512, 1980.

[46] A. Brusilovsky, "Mathematical simulation of phase behavior of natural multicomponent systems at high pressures with an equation of state," *SPE Reservoir Engineering*, vol. 7, no. 1, pp. 117–122, 1992.

[47] C. Tsallis, "Possible generalization of Boltzmann-Gibbs statistics," *Journal of Statistical Physics*, vol. 52, no. 1-2, pp. 479–487, 1988.

[48] C. Tsallis, "Nonextensive statistics: theoretical, experimental and computational evidences and connections," *Brazilian Journal of Physics*, vol. 29, no. 1, pp. 1–35, 1999.

[49] M. Schoen and D. J. Diestler, "Analytical treatment of a simple fluid adsorbed in a slit-pore," *The Journal of Chemical Physics*, vol. 109, no. 13, pp. 5596–5606, 1998.

[50] M. Rezaveisi, K. Sepehrnoori, G. A. Pope, and R. T. Johns, "Compositional simulation including effect of capillary pressure on phase behavior," in *SPE Annual Technical Conference and Exhibition*, Houston, Texas, USA, September 2015.

[51] K. Morishige, H. Fujii, M. Uga, and D. Kinukawa, "Capillary critical point of argon, nitrogen, oxygen, ethylene, and carbon dioxide in MCM-41," *Langmuir*, vol. 13, no. 13, pp. 3494–3498, 1997.

[52] K. Morishige and M. Shikimi, "Adsorption hysteresis and pore critical temperature in a single cylindrical pore," *The Journal of Chemical Physics*, vol. 108, no. 18, pp. 7821–7824, 1998.

[53] G. J. Zarragoicoechea and V. A. Kuz, "Critical shift of a confined fluid in a nanopore," *Fluid Phase Equilibria*, vol. 220, no. 1, pp. 7–9, 2004.

[54] S. K. Singh, A. Sinha, G. Deo, and J. K. Singh, "Vapor– liquid phase coexistence, critical properties, and surface tension of confined alkanes," *The Journal of Physical Chemistry C*, vol. 113, no. 17, pp. 7170–7180, 2009.

[55] K. Sapmanee, *Effects of Pore Proximity on Behavior and Production Prediction of Gas/Condensate*, University of Oklahoma, 2011.

[56] D. Devegowda, K. Sapmanee, F. Civan, and R. F. Sigal, "Phase behavior of gas condensates in shales due to pore proximity effects: implications for transport, reserves and well productivity," in *SPE Annual Technical Conference and Exhibition*, San Antonio, Texas, USA, October 2012.

[57] N. S. Alharthy, T. N. Nguyen, T. W. Teklu, H. Kazemi, and R. M. Graves, "Multiphase compositional modeling in small-scale pores of unconventional shale reservoirs," in *SPE Annual Technical Conference and Exhibition*, New Orleans, Louisiana, USA, September 2013.

[58] L. Jin, Y. Ma, and A. Jamili, "Investigating the effect of pore proximity on phase behavior and fluid properties in shale formations," in *SPE Annual Technical Conference and Exhibition*, New Orleans, Louisiana, USA, September 2013.

[59] Y. Zhang, W. Yu, K. Sepehrnoori, and Y. Di, "Investigation of nanopore confinement on fluid flow in tight reservoirs," *Journal of Petroleum Science and Engineering*, vol. 150, pp. 265–271, 2017.

[60] P. B. Balbuena and K. E. Gubbins, "Theoretical interpretation of adsorption behavior of simple fluids in slit pores," *Langmuir*, vol. 9, no. 7, pp. 1801–1814, 1993.

[61] M. Sedghi, L. Goual, W. Welch, and J. Kubelka, "Effect of asphaltene structure on association and aggregation using molecular dynamics," *The Journal of Physical Chemistry B*, vol. 117, no. 18, pp. 5765–5776, 2013.

[62] A. Vishnyakov, E. Piotrovskaya, E. Brodskaya, E. V. Votyakov, and Y. K. Tovbin, "Critical properties of Lennard-Jones fluids in narrow slit-shaped pores," *Langmuir*, vol. 17, no. 14, pp. 4451–4458, 2001.

[63] S. K. Singh and J. K. Singh, "Effect of pore morphology on vapor-liquid phase transition and crossover behavior of critical properties from 3D to 2D," *Fluid Phase Equilibria*, vol. 300, no. 1-2, pp. 182–187, 2011.

[64] A. W. Islam, T. W. Patzek, and A. Y. Sun, "Thermodynamics phase changes of nanopore fluids," *Journal of Natural Gas Science and Engineering*, vol. 25, pp. 134–139, 2015.

[65] L. Travalloni, M. Castier, F. W. Tavares, and S. I. Sandler, "Thermodynamic modeling of confined fluids using an extension of the generalized van der Waals theory," *Chemical Engineering Science*, vol. 65, no. 10, pp. 3088–3099, 2010.

[66] A. A. Ibrahim, *Effect of Pore Size Distribution on Multiphase Equilibrium of Fluids Confined in Porous Media*, Texas A & M University, 2016.

[67] S. Luo, J. L. Lutkenhaus, and H. Nasrabadi, "Confinement-induced supercriticality and phase equilibria of hydrocarbons in nanopores," *Langmuir*, vol. 32, no. 44, pp. 11506–11513, 2016.

[68] S. Luo, J. L. Lutkenhaus, and H. Nasrabadi, "Use of differential scanning calorimetry to study phase behavior of hydrocarbon mixtures in nano-scale porous media," *Journal of Petroleum Science and Engineering*, vol. 163, pp. 731–738, 2018.

[69] S. Li, M. Dong, Z. Li, S. Huang, H. Qing, and E. Nickel, "Gas breakthrough pressure for hydrocarbon reservoir seal rocks: implications for the security of long-term CO2 storage in the Weyburn field," *Geofluids*, vol. 5, no. 4, p. 334, 2005.

[70] Q.-Y. Ren, G.-J. Chen, W. Yan, and T.-M. Guo, "Interfacial tension of (CO2+ CH4)+ water from 298 K to 373 K and pressures up to 30 MPa," *Journal of Chemical & Engineering Data*, vol. 45, no. 4, pp. 610–612, 2000.

[71] C. Chao, G. Xu, and X. Fan, "Effect of surface tension, viscosity, pore geometry and pore contact angle on effective pore throat," *Chemical Engineering Science*, vol. 197, pp. 269–279, 2019.

[72] L. M. Pereira, A. Chapoy, R. Burgass, and B. Tohidi, "Interfacial tension of CO_2 + brine systems: experiments and predictive modelling," *Advances in Water Resources*, vol. 103, pp. 64–75, 2017.

[73] S. Bachu and B. Bennion, "Effects of in-situ conditions on relative permeability characteristics of CO2-brine systems," *Environmental Geology*, vol. 54, no. 8, pp. 1707–1722, 2008.

[74] C. Aggelopoulos, M. Robin, and O. Vizika, "Interfacial tension between CO_2 and brine (NaCl + $CaCl_2$) at elevated pressures and temperatures: the additive effect of different salts," *Advances in Water Resources*, vol. 34, no. 4, pp. 505–511, 2011.

[75] C. Chalbaud, M. Robin, J.-M. Lombard, H. Bertin, and P. Egermann, "Brine/CO2interfacial properties and effects

on CO2storage in deep saline aquifers," *Oil & Gas Science and Technology–Revue de l'Institut Français du Pétrole*, vol. 65, no. 4, pp. 541–555, 2010.

[76] Y. Liu, H. A. Li, and R. Okuno, "Measurements and modeling of interfacial tension for CO2/CH4/brine systems under reservoir conditions," *Industrial & Engineering Chemistry Research*, vol. 55, no. 48, pp. 12358–12375, 2016.

[77] D. B. Bennion and S. Bachu, "Dependence on temperature, pressure, and salinity of the IFT and relative permeability displacement characteristics of CO2 injected in deep saline aquifers," in *SPE Annual Technical Conference and Exhibition*, San Antonio, Texas, USA, September 2006.

[78] X. Li, E. S. Boek, G. C. Maitland, and J. P. M. Trusler, "Interfacial tension of (brines + CO_2): $CaCl_2$(aq), $MgCl_2$(aq), and Na_2SO_4(aq) at temperatures between (343 and 423) K, pressures between (2 and 50) MPa, and molalities of (0.5 to 5) mol·kg^{-1}," *Journal of Chemical & Engineering Data*, vol. 57, no. 5, pp. 1369–1375, 2012.

[79] M. Mutailipu, Y. Liu, L. Jiang, and Y. Zhang, "Measurement and estimation of CO_2-brine interfacial tension and rock wettability under CO_2 sub- and super- critical conditions," *Journal of colloid and interface science*, vol. 534, pp. 605–617, 2019.

[80] A. Firoozabadi and H. J. Ramey Jr., "Surface tension of water-hydrocarbon systems at reservoir conditions," *Journal of Canadian Petroleum Technology*, vol. 27, no. 3, 1988.

[81] M. J. Argaud, "Predicting the interfacial tension of brine/gas (or condensate) systems," in *Advances in core evaluation III reservoir management*, pp. 147–174, Taylor & Francis, London, 1993.

[82] R. P. Sutton, "An improved model for water-hydrocarbon surface tension at reservoir conditions," in *SPE Annual Technical Conference and Exhibition*, New Orleans, Louisiana, October 2009.

[83] C. Chalbaud, M. Robin, J.-M. Lombard, F. Martin, P. Egermann, and H. Bertin, "Interfacial tension measurements and wettability evaluation for geological CO_2 storage," *Advances in Water Resources*, vol. 32, no. 1, pp. 98–109, 2009.

[84] L. C. Nielsen, I. C. Bourg, and G. Sposito, "Predicting CO_2-water interfacial tension under pressure and temperature conditions of geologic CO_2 storage," *Geochimica et Cosmochimica Acta*, vol. 81, pp. 28–38, 2012.

[85] A. Silvestri, E. Ataman, A. Budi, S. L. S. Stipp, J. D. Gale, and P. Raiteri, "Wetting properties of the CO2–water–calcite system via molecular simulations: shape and size effects," *Langmuir*, vol. 35, no. 50, pp. 16669–16678, 2019.

[86] P. Chiquet, J.-L. Daridon, D. Broseta, and S. Thibeau, "CO_2/water interfacial tensions under pressure and temperature conditions of CO_2 geological storage," *Energy Conversion and Management*, vol. 48, no. 3, pp. 736–744, 2007.

[87] H. Zhang, S. Chen, Z. Guo, Y. Liu, F. Bresme, and X. Zhang, "Contact line pinning effects influence determination of the line tension of droplets adsorbed on substrates," *The Journal of Physical Chemistry C*, vol. 122, no. 30, pp. 17184–17189, 2018.

[88] D. N. Espinoza and J. C. Santamarina, "Water-CO2-mineral systems: interfacial tension, contact angle, and diffusion—Implications to CO2geological storage," *Water Resources Research*, vol. 46, no. 7, 2010.

[89] S. Wang, I. M. Edwards, and A. F. Clarens, "Wettability phenomena at the CO2–brine–mineral interface: implications for geologic carbon sequestration," *Environmental Science & Technology*, vol. 47, no. 1, pp. 234–241, 2012.

[90] M. Arif, M. Lebedev, A. Barifcani, and S. Iglauer, "CO_2 storage in carbonates: wettability of calcite," *International Journal of Greenhouse Gas Control*, vol. 62, pp. 113–121, 2017.

[91] M. P. Andersson, K. Dideriksen, H. Sakuma, and S. L. S. Stipp, "Modelling how incorporation of divalent cations affects calcite wettability- implications for biomineralisation and oil recovery," *Scientific Reports*, vol. 6, no. 1, p. 28854, 2016.

[92] N. Bovet, M. Yang, M. S. Javadi, and S. L. S. Stipp, "Interaction of alcohols with the calcite surface," *Physical Chemistry Chemical Physics*, vol. 17, no. 5, pp. 3490–3496, 2015.

[93] S. S. Hakim, M. H. M. Olsson, H. O. Sørensen et al., "Interactions of the calcite {10.4} surface with organic compounds: structure and behaviour at mineral–organic interfaces," *Scientific Reports*, vol. 7, no. 1, pp. 1–11, 2017.

[94] H. Wang, V. Alfredsson, J. Tropsch, R. Ettl, and T. Nylander, "Formation of $CaCO_3$ deposits on hard surfaces effect of bulk solution conditions and surface properties," *ACS Applied Materials & Interfaces*, vol. 5, no. 10, pp. 4035–4045, 2013.

[95] F. Gray, B. Anabaraonye, S. Shah, E. Boek, and J. Crawshaw, "Chemical mechanisms of dissolution of calcite by HCl in porous media: simulations and experiment," *Advances in Water Resources*, vol. 121, pp. 369–387, 2018.

[96] S. C. Ayirala and D. N. Rao, "Comparative evaluation of a new gas/oil miscibility-determination technique," *Journal of Canadian Petroleum Technology*, vol. 50, no. 9, pp. 71–81, 2011.

[97] Y. Zhang, H. Liu, W. Li et al., "Intraflagellar transporter protein (IFT27), an IFT25 binding partner, is essential for male fertility and spermiogenesis in mice," *Developmental Biology*, vol. 432, no. 1, pp. 125–139, 2017.

[98] K. Zhang and Y. Gu, "Two new quantitative technical criteria for determining the minimum miscibility pressures (MMPs) from the vanishing interfacial tension (VIT) technique," *Fuel*, vol. 184, pp. 136–144, 2016.

[99] D. N. Rao, "A new technique of vanishing interfacial tension for miscibility determination," *Fluid Phase Equilibria*, vol. 139, no. 1-2, pp. 311–324, 1997.

[100] C. H. Whitson and M. R. Brulé, "Phase behavior," in *Henry L. Doherty Memorial Fund of AIME*, Society of Petroleum Engineers, 2000.

[101] P. Dong, M. Puerto, G. Jian et al., "Exploring low-IFT foam EOR in fractured carbonates: success and particular challenges of sub-10-mD limestone," *SPE Journal*, vol. 25, no. 2, 2020.

[102] R. Goetz and R. Lipowsky, "Computer simulations of bilayer membranes: self-assembly and interfacial tension," *The Journal of Chemical Physics*, vol. 108, no. 17, pp. 7397–7409, 1998.

[103] F. Goujon, A. Dequidt, A. Ghoufi, and P. Malfreyt, "How does the surface tension depend on the surface area with coarse-grained models?," *Journal of Chemical Theory and Computation*, vol. 14, no. 5, pp. 2644–2651, 2018.

[104] T. W. Teklu, N. Alharthy, H. Kazemi, X. Yin, and R. M. Graves, "Vanishing interfacial tension algorithm for MMP determination in unconventional reservoirs," in *SPE Western North American and Rocky Mountain Joint Meeting*, Denver, Colorado, April 2014.

[105] K. Zhang, N. Jia, S. Li, and L. Liu, "Nanoscale-extended correlation to calculate gas solvent minimum miscibility

pressures in tight oil reservoirs," *Journal of Petroleum Science and Engineering*, vol. 171, pp. 1455–1465, 2018.

[106] L. Li and J. J. Sheng, "Nanopore confinement effects on phase behavior and capillary pressure in a Wolfcamp shale reservoir," *Journal of the Taiwan Institute of Chemical Engineers*, vol. 78, pp. 317–328, 2017.

[107] M. K. Emera and H. K. Sarma, "Use of genetic algorithm to estimate CO_2-oil minimum miscibility pressure–a key parameter in design of CO_2 miscible flood," *Journal of Petroleum Science and Engineering*, vol. 46, no. 1-2, pp. 37–52, 2005.

[108] F. Du, B. Nojabaei, and R. T. Johns, "A black-oil approach to model produced gas injection for enhanced recovery of conventional and unconventional reservoirs," in *SPE Annual Technical Conference and Exhibition*, Dallas, Texas, USA, September 2018.

[109] K. Zhang, B. Nojabaei, K. Ahmadi, and R. T. Johns, "Minimum miscibility pressure calculation for oil shale and tight reservoirs with large gas-oil capillary pressure," in *Unconventional Resources Technology Conference (URTEC)*, Houston, Texas, USA, July 2018.

[110] S. Wang, M. Ma, and S. Chen, "Application of PC-SAFT equation of state for CO 2 minimum miscibility pressure prediction in nanopores," in *SPE Improved Oil Recovery Conference*, Tulsa, Oklahoma, USA, April 2016.

[111] J. Huang, T. Jin, Z. Chai, M. Barrufet, and J. Killough, "Compositional simulation of fractured shale reservoir with distribution of nanopores using coupled multi-porosity and EDFM method," *Journal of Petroleum Science and Engineering*, vol. 179, pp. 1078–1089, 2019.

[112] Q. Kang, P. C. Lichtner, H. S. Viswanathan, and A. I. Abdel-Fattah, "Pore scale modeling of reactive transport involved in geologic CO 2 sequestration," *Transport in Porous Media*, vol. 82, no. 1, pp. 197–213, 2010.

[113] H. P. Menke, B. Bijeljic, M. G. Andrew, and M. J. Blunt, "Dynamic three-dimensional pore-scale imaging of reaction in a carbonate at reservoir conditions," *Environmental Science & Technology*, vol. 49, no. 7, pp. 4407–4414, 2015.

[114] T. Ajayi, J. S. Gomes, and A. Bera, "A review of CO 2 storage in geological formations emphasizing modeling, monitoring and capacity estimation approaches," *Petroleum Science*, vol. 16, no. 5, pp. 1028–1063, 2019.

[115] A.-H. A. Park and L.-S. Fan, "CO2 mineral sequestration: physically activated dissolution of serpentine and pH swing process," *Chemical Engineering Science*, vol. 59, no. 22-23, pp. 5241–5247, 2004.

[116] V. N. Balashov, G. D. Guthrie, J. A. Hakala, C. L. Lopano, J. D. Rimstidt, and S. L. Brantley, "Predictive modeling of CO_2 sequestration in deep saline sandstone reservoirs: Impacts of geochemical kinetics," *Applied Geochemistry*, vol. 30, pp. 41–56, 2013.

[117] M. Knackstedt and X. Zhang, "Direct evaluation of length scales and structural parameters associated with flow in porous media," *Physical Review E*, vol. 50, no. 3, pp. 2134–2138, 1994.

[118] E. Moreira and J. Coury, "The influence of structural parameters on the permeability of ceramic foams," *Brazilian Journal of Chemical Engineering*, vol. 21, no. 1, pp. 23–33, 2004.

[119] L. Algive, S. Bekri, and O. Vizika, "Pore-network modeling dedicated to the determination of the petrophysical-property changes in the presence of reactive fluid," *SPE Journal*, vol. 15, no. 3, pp. 618–633, 2010.

[120] D. Wang, J. Yao, Z. Chen, W. Song, and H. Sun, "Image-based core-scale real gas apparent permeability from pore-scale experimental data in shale reservoirs," *Fuel*, vol. 254, article 115596, 2019.

[121] G. Sheng, Y. Su, and W. Wang, "A new fractal approach for describing induced-fracture porosity/permeability/compressibility in stimulated unconventional reservoirs," *Journal of Petroleum Science and Engineering*, vol. 179, pp. 855–866, 2019.

[122] M. Cai, D. Elsworth, Y. Su, and M. Lu, "A new fractal temporal conductivity model for propped fracture and its application in tight reservoirs," *Fractals*, vol. 28, no. 5, article 2050074, 2020.

[123] A. Navarre-Sitchler, C. I. Steefel, L. Yang, L. Tomutsa, and S. L. Brantley, "Evolution of porosity and diffusivity associated with chemical weathering of a basalt clast," *Journal of Geophysical Research: Earth Surface*, vol. 114, no. F2, 2009.

[124] N. Nishiyama and T. Yokoyama, "Permeability of porous media: role of the critical pore size," *Journal of Geophysical Research: Solid Earth*, vol. 122, no. 9, pp. 6955–6971, 2017.

[125] C. Noiriel, P. Gouze, and B. Made, "3D analysis of geometry and flow changes in a limestone fracture during dissolution," *Journal of hydrology*, vol. 486, pp. 211–223, 2013.

[126] S. Emmanuel and Y. Levenson, "Limestone weathering rates accelerated by micron-scale grain detachment," *Geology*, vol. 42, no. 9, pp. 751–754, 2014.

[127] H. Deng, C. Steefel, S. Molins, and D. DePaolo, "Fracture evolution in multimineral systems: the role of mineral composition, flow rate, and fracture aperture heterogeneity," *ACS Earth and Space Chemistry*, vol. 2, no. 2, pp. 112–124, 2018.

[128] M. Garcia-Rios, L. Luquot, J. M. Soler, and J. Cama, "Influence of the flow rate on dissolution and precipitation features during percolation of CO2-rich sulfate solutions through fractured limestone samples," *Chemical Geology*, vol. 414, pp. 95–108, 2015.

[129] G. Dávila, L. Luquot, J. M. Soler, and J. Cama, "Interaction between a fractured marl caprock and CO2-rich sulfate solution under supercritical CO2 conditions," *International Journal of Greenhouse Gas Control*, vol. 48, pp. 105–119, 2016.

[130] Y. Bernabé, U. Mok, B. Evans, and F. J. Herrmann, "Permeability and storativity of binary mixtures of high-and low-permeability materials," *Journal of Geophysical Research: Solid Earth*, vol. 109, no. B12, 2004.

[131] C. Noiriel, P. Gouze, and D. Bernard, "Investigation of porosity and permeability effects from microstructure changes during limestone dissolution," *Geophysical Research Letters*, vol. 31, no. 24, 2004.

[132] C. Meile and K. Tuncay, "Scale dependence of reaction rates in porous media," *Advances in Water Resources*, vol. 29, no. 1, pp. 62–71, 2006.

[133] L. Li, C. I. Steefel, and L. Yang, "Scale dependence of mineral dissolution rates within single pores and fractures," *Geochimica et Cosmochimica Acta*, vol. 72, no. 2, pp. 360–377, 2008.

[134] R. Shiraki and T. L. Dunn, "Experimental study on water–rock interactions during CO2 flooding in the Tensleep Formation, Wyoming, USA," *Applied Geochemistry*, vol. 15, no. 3, pp. 265–279, 2000.

[135] N. Muller, R. Qi, E. Mackie, K. Pruess, and M. J. Blunt, "CO2 injection impairment due to halite precipitation," *Energy Procedia*, vol. 1, no. 1, pp. 3507–3514, 2009.

[136] G. D. Ross, A. C. Todd, J. A. Tweedie, and A. G. Will, "The dissolution effects of CO2-brine systems on the permeability

of UK and North Sea calcareous sandstones," in *SPE enhanced oil recovery symposium*, Tulsa, Oklahoma, April 1982.

[137] T. Rathnaweera, P. Ranjith, and M. Perera, "Experimental investigation of geochemical and mineralogical effects of CO 2 sequestration on flow characteristics of reservoir rock in deep saline aquifers," *Scientific Reports*, vol. 6, article 19362, 2016.

[138] B. L. Alemu, P. Aagaard, I. A. Munz, and E. Skurtveit, "Caprock interaction with CO2: a laboratory study of reactivity of shale with supercritical CO2 and brine," *Applied Geochemistry*, vol. 26, no. 12, pp. 1975–1989, 2011.

[139] C. J. Werth, C. Zhang, M. L. Brusseau, M. Oostrom, and T. Baumann, "A review of non-invasive imaging methods and applications in contaminant hydrogeology research," *Journal of contaminant hydrology*, vol. 113, no. 1-4, pp. 1–24, 2010.

[140] S. Molins, D. Trebotich, L. Yang et al., "Pore-scale controls on calcite dissolution rates from flow-through laboratory and numerical experiments," *Environmental science & technology*, vol. 48, no. 13, pp. 7453–7460, 2014.

[141] P. Meakin and A. M. Tartakovsky, "Modeling and simulation of pore-scale multiphase fluid flow and reactive transport in fractured and porous media," *Reviews of Geophysics*, vol. 47, no. 3, 2009.

[142] Y. Han and P. A. Cundall, "Lattice Boltzmann modeling of pore-scale fluid flow through idealized porous media," *International Journal for Numerical Methods in Fluids*, vol. 67, no. 11, pp. 1720–1734, 2011.

[143] B. Ahrenholz, J. Tölke, P. Lehmann et al., "Prediction of capillary hysteresis in a porous material using lattice-Boltzmann methods and comparison to experimental data and a morphological pore network model," *Advances in Water Resources*, vol. 31, no. 9, pp. 1151–1173, 2008.

[144] A. M. Tartakovsky and P. Meakin, "Pore scale modeling of immiscible and miscible fluid flows using smoothed particle hydrodynamics," *Advances in Water Resources*, vol. 29, no. 10, pp. 1464–1478, 2006.

[145] J. Dewanckele, T. De Kock, M. Boone et al., "4D imaging and quantification of pore structure modifications inside natural building stones by means of high resolution X-ray CT," *Science of the total environment*, vol. 416, pp. 436–448, 2012.

[146] J. Vilcáez, S. Morad, and N. Shikazono, "Pore-scale simulation of transport properties of carbonate rocks using FIB-SEM 3D microstructure: implications for field scale solute transport simulations," *Journal of Natural Gas Science and Engineering*, vol. 42, pp. 13–22, 2017.

[147] J. Pereira Nunes, M. Blunt, and B. Bijeljic, "Pore-scale simulation of carbonate dissolution in micro-CT images," *Journal of Geophysical Research: Solid Earth*, vol. 121, no. 2, pp. 558–576, 2016.

[148] Z. Tian and J. Wang, "Lattice Boltzmann simulation of dissolution-induced changes in permeability and porosity in 3D CO2 reactive transport," *Journal of Hydrology*, vol. 557, pp. 276–290, 2018.

[149] H. Deng, S. Molins, C. Steefel et al., "A 2.5 D reactive transport model for fracture alteration simulation," *Environmental Science & Technology*, vol. 50, no. 14, pp. 7564–7571, 2016.

[150] C. I. Steefel, S. Molins, and D. Trebotich, "Pore scale processes associated with subsurface CO2 injection and sequestration," *Reviews in Mineralogy and Geochemistry*, vol. 77, no. 1, pp. 259–303, 2013.

[151] L. Li, C. A. Peters, and M. A. Celia, "Upscaling geochemical reaction rates using pore-scale network modeling," *Advances in Water Resources*, vol. 29, no. 9, pp. 1351–1370, 2006.

[152] A. Raoof, S. M. Hassanizadeh, and A. Leijnse, "Upscaling transport of adsorbing solutes in porous media: pore-network modeling," *Vadose Zone Journal*, vol. 9, no. 3, pp. 624–636, 2010.

[153] J. Tansey and M. T. Balhoff, "Pore network modeling of reactive transport and dissolution in porous media," *Transport in Porous Media*, vol. 113, no. 2, pp. 303–327, 2016.

[154] C. Varloteaux, S. Békri, and P. M. Adler, "Pore network modelling to determine the transport properties in presence of a reactive fluid: from pore to reservoir scale," *Advances in Water Resources*, vol. 53, pp. 87–100, 2013.

[155] H. Dong and M. J. Blunt, "Pore-network extraction from micro-computerized-tomography images," *Physical Review E*, vol. 80, no. 3, article 036307, 2009.

[156] Q. Kang, P. C. Lichtner, and D. Zhang, "Lattice Boltzmann pore-scale model for multicomponent reactive transport in porous media," *Journal of Geophysical Research: Solid Earth*, vol. 111, no. B5, 2006.

[157] A. Parmigiani, *Lattice Boltzmann calculations of reactive multiphase Flows in Porous Media*, University of Geneva, 2011.

[158] S. Molins, D. Trebotich, C. I. Steefel, and C. Shen, "An investigation of the effect of pore scale flow on average geochemical reaction rates using direct numerical simulation," *Water Resources Research*, vol. 48, no. 3, 2012.

[159] L. Chen, Q. Kang, B. Carey, and W. Q. Tao, "Pore-scale study of diffusion–reaction processes involving dissolution and precipitation using the lattice Boltzmann method," *International Journal of Heat and Mass Transfer*, vol. 75, pp. 483–496, 2014.

[160] Q. Kang, L. Chen, A. J. Valocchi, and H. S. Viswanathan, "Pore-scale study of dissolution-induced changes in permeability and porosity of porous media," *Journal of Hydrology*, vol. 517, pp. 1049–1055, 2014.

[161] L. Chen, Q. Kang, Q. Tang, B. A. Robinson, Y. L. He, and W. Q. Tao, "Pore-scale simulation of multicomponent multiphase reactive transport with dissolution and precipitation," *International Journal of Heat and Mass Transfer*, vol. 85, pp. 935–949, 2015.

[162] S. Zendehboudi, A. Shafiei, A. Bahadori, L. A. James, A. Elkamel, and A. Lohi, "Asphaltene precipitation and deposition in oil reservoirs–technical aspects, experimental and hybrid neural network predictive tools," *Chemical Engineering Research and Design*, vol. 92, no. 5, pp. 857–875, 2014.

[163] K. J. Leontaritis and G. A. Mansoori, "Asphaltene deposition: a survey of field experiences and research approaches," *Journal of Petroleum Science and Engineering*, vol. 1, no. 3, pp. 229–239, 1988.

[164] L. X. Nghiem and D. A. Coombe, "Modelling asphaltene precipitation during primary depletion," *SPE Journal*, vol. 2, no. 2, pp. 170–176, 1997.

[165] H. R. Ansari and A. Gholami, "Robust method based on optimized support vector regression for modeling of asphaltene precipitation," *Journal of Petroleum Science and Engineering*, vol. 135, pp. 201–205, 2015.

[166] M. Haghshenasfard and K. Hooman, "CFD modeling of asphaltene deposition rate from crude oil," *Journal of Petroleum Science and Engineering*, vol. 128, pp. 24–32, 2015.

[167] H. Seyyedbagheri and B. Mirzayi, "CFD modeling of high inertia asphaltene aggregates deposition in 3D turbulent oil

production wells," *Journal of Petroleum Science and Engineering*, vol. 150, pp. 257–264, 2017.

[168] S. Yaseen and G. A. Mansoori, "Asphaltene aggregation due to waterflooding (a molecular dynamics study)," *Journal of Petroleum Science and Engineering*, vol. 170, pp. 177–183, 2018.

[169] D. L. Gonzalez, F. M. Vargas, G. J. Hirasaki, and W. G. Chapman, "Modeling study of CO2-induced asphaltene precipitation," *Energy & Fuels*, vol. 22, no. 2, pp. 757–762, 2008.

[170] K. J. Leontaritis, "The asphaltene and wax deposition envelopes," *Fuel Science and Technology International*, vol. 14, no. 1-2, pp. 13–39, 1996.

[171] D. L. Gonzalez, E. Mahmoodaghdam, F. H. Lim, and N. B. Joshi, "Effects of gas additions to deepwater gulf of mexico reservoir oil: experimental investigation of asphaltene precipitation and deposition," in *SPE Annual Technical Conference and Exhibition*, San Antonio, Texas, USA, October 2012.

[172] A. Jamaluddin, J. Creek, C. Kabir et al., "Laboratory techniques to measure thermodynamic asphaltene instability," *Journal of Canadian Petroleum Technology*, vol. 41, no. 7, 2002.

[173] S. Moradi, M. Dabiri, B. Dabir, D. Rashtchian, and M. A. Emadi, "Investigation of asphaltene precipitation in miscible gas injection processes: experimental study and modeling," *Brazilian Journal of Chemical Engineering*, vol. 29, no. 3, pp. 665–676, 2012.

[174] S. Negahban, J. Bahamaish, N. Joshi, J. Nighswander, and A. K. M. Jamaluddin, "An experimental study at an Abu Dhabi reservoir of asphaltene precipitation caused by gas injection," *SPE Production & Facilities*, vol. 20, no. 2, pp. 115–125, 2005.

[175] T. Jafari Behbahani, C. Ghotbi, V. Taghikhani, and A. Shahrabadi, "Asphaltene deposition under dynamic conditions in porous media: theoretical and experimental investigation," *Energy & fuels*, vol. 27, no. 2, pp. 622–639, 2013.

[176] A. M. Kalantari-Dahaghi, J. Moghadasi, V. Gholami, and R. Abdi, "Formation damage due to asphaltene precipitation resulting from CO2 gas injection in Iranian carbonate reservoirs," in *SPE Europec/EAGE Annual Conference and Exhibition*, Vienna, Austria, June 2006.

[177] J. Liu, Y. Zhao, and S. Ren, "Molecular dynamics simulation of self-aggregation of asphaltenes at an oil/water interface: formation and destruction of the asphaltene protective film," *Energy & Fuels*, vol. 29, no. 2, pp. 1233–1242, 2015.

[178] E. Rogel, "Studies on asphaltene aggregation via computational chemistry," *Colloids and Surfaces A: Physicochemical and Engineering Aspects*, vol. 104, no. 1, pp. 85–93, 1995.

[179] E. Lowry, M. Sedghi, and L. Goual, "Polymers for asphaltene dispersion: interaction mechanisms and molecular design considerations," *Journal of Molecular Liquids*, vol. 230, pp. 589–599, 2017.

[180] S. T. Kim, M.-E. Boudh-Hir, and G. A. Mansoori, "The Role of Asphaltene in Wettability Reversal," in *SPE Annual Technical Conference and Exhibition*, New Orleans, Louisiana, September 1990.

[181] T. Monger and J. Fu, "The Nature of CO2-Induced Organic Deposition," in *SPE Annual Technical Conference and Exhibition*, Dallas, Texas, September 1987.

[182] H. Rassamdana, B. Dabir, M. Nematy, M. Farhani, and M. Sahimi, "Asphalt flocculation and deposition: I. The onset of precipitation," *AIChE Journal*, vol. 42, no. 1, pp. 10–22, 1996.

[183] S. Soroush, P. Pourafshary, and M. Vafaie-Sefti, "A comparison of asphaltene deposition in miscible and immiscible carbon dioxide flooding in porous media," in *SPE EOR Conference at Oil and Gas West Asia*, Muscat, Oman, March 2014.

[184] R. K. Srivastava and S. S. Huang, "Asphaltene Deposition during CO2 Flooding: A Laboratory Assessment," in *SPE Production Operations Symposium*, Oklahoma City, Oklahoma, March 1997.

[185] R. Srivastava, S. Huang, and M. Dong, "Asphaltene deposition during CO2 flooding," *SPE production & facilities*, vol. 14, no. 4, pp. 235–245, 1999.

[186] T. Headen, E. Boek, G. Jackson, T. S. Totton, and E. A. Müller, "Simulation of asphaltene aggregation through molecular dynamics: insights and limitations," *Energy & Fuels*, vol. 31, no. 2, pp. 1108–1125, 2017.

[187] J. Wang and A. L. Ferguson, "Mesoscale simulation of asphaltene aggregation," *The Journal of Physical Chemistry B*, vol. 120, no. 32, pp. 8016–8035, 2016.

[188] J. Costa, D. Simionesie, Z. Zhang, and P. A. Mulheran, "Aggregation of model asphaltenes: a molecular dynamics study," *Journal of Physics: Condensed Matter*, vol. 28, no. 39, article 394002, 2016.

[189] M. Mehana, J. Abraham, and M. Fahes, "The impact of asphaltene deposition on fluid flow in sandstone," *Journal of Petroleum Science and Engineering*, vol. 174, pp. 676–681, 2019.

[190] S. M. Fakher, *Asphaltene Stability in Crude Oil during Carbon Dioxide Injection and Its Impact on Oil Recovery: A Review, Data Analysis, and Experimental Study*, Missouri University of Science and Technology, 2019.

[191] R. Hamadou, M. Khodja, M. Kartout, and A. Jada, "Permeability reduction by asphaltenes and resins deposition in porous media," *Fuel*, vol. 87, no. 10-11, pp. 2178–2185, 2008.

[192] R. S. Al-Maamari and J. S. Buckley, "Asphaltene precipitation and alteration of wetting: the potential for wettability changes during oil production," *SPE Reservoir Evaluation & Engineering*, vol. 6, no. 4, pp. 210–214, 2003.

[193] M. I. Mohamed and V. Alvarado, "Smart water flooding in Berea sandstone at low temperature: is wettability alteration the sole mechanism at play?," in *SPE Annual Technical Conference and Exhibition*, San Antonio, Texas, USA, October 2017.

[194] R. T. Okwen, "Formation damage by CO2 asphaltene precipitation," in *SPE International Symposium and Exhibition on Formation Damage Control*, Lafayette, Louisiana, USA, February 2006.

[195] R. S. Mohammad, S. Zhang, S. Lu, S. Jamal-Ud-Din, and X. Zhao, "Simulation study of asphaltene deposition and solubility of CO2 in the brine during cyclic CO2 injection process in unconventional tight reservoirs," *International Journal of Geological and Environmental Engineering*, vol. 11, no. 6, pp. 495–510, 2017.

[196] Z. Shen and J. J. Sheng, "Experimental and numerical study of permeability reduction caused by asphaltene precipitation and deposition during CO2 huff and puff injection in Eagle Ford shale," *Fuel*, vol. 211, pp. 432–445, 2018.

[197] S. Fakher and A. Imqam, "Asphaltene precipitation and deposition during CO2 injection in nano shale pore structure and its impact on oil recovery," *Fuel*, vol. 237, pp. 1029–1039, 2019.

[198] H. Sun, H. Zhao, N. Qi, K. Zhang, Q. Wang, and Y. Li, "Competitive adsorption of CO2 over N2 in asphaltene slit nanopores studied by molecular simulation," *Energy & Fuels*, vol. 31, no. 12, pp. 13979–13984, 2017.

[199] K. Pruess and J. Garcia, "Multiphase flow dynamics during CO 2 disposal into saline aquifers," *Environmental Geology*, vol. 42, no. 2-3, pp. 282–295, 2002.

[200] J. M. Nordbotten, M. A. Celia, and S. Bachu, "Injection and storage of CO 2 in deep saline aquifers: analytical solution for CO 2 plume evolution during injection," *Transport in Porous media*, vol. 58, no. 3, pp. 339–360, 2005.

[201] R. Juanes, E. J. Spiteri, F. M. Orr Jr., and M. J. Blunt, "Impact of relative permeability hysteresis on geological CO2 storage," *Water Resources Research*, vol. 42, no. 12, 2006.

[202] E. Mouche, M. Hayek, and C. Mügler, "Upscaling of CO2 vertical migration through a periodic layered porous medium: The capillary-free and capillary-dominant cases," *Advances in Water Resources*, vol. 33, no. 9, pp. 1164–1175, 2010.

[203] J. Rutqvist, Y.-S. Wu, C.-F. Tsang, and G. Bodvarsson, "A modeling approach for analysis of coupled multiphase fluid flow, heat transfer, and deformation in fractured porous rock," *International Journal of Rock Mechanics and Mining Sciences*, vol. 39, no. 4, pp. 429–442, 2002.

[204] F. Cappa and J. Rutqvist, "Modeling of coupled deformation and permeability evolution during fault reactivation induced by deep underground injection of CO2," *International Journal of Greenhouse Gas Control*, vol. 5, no. 2, pp. 336–346, 2011.

[205] C. Ehlig-Economides and M. J. Economides, "Sequestering carbon dioxide in a closed underground volume," *Journal of Petroleum Science and Engineering*, vol. 70, no. 1-2, pp. 123–130, 2010.

[206] G. Sheng, H. Zhao, Y. Su et al., "An analytical model to couple gas storage and transport capacity in organic matter with noncircular pores," *Fuel*, vol. 268, article 117288, 2020.

[207] J. T. Birkholzer, C. M. Oldenburg, and Q. Zhou, "CO2 migration and pressure evolution in deep saline aquifers," *International Journal of Greenhouse Gas Control*, vol. 40, pp. 203–220, 2015.

[208] J. T. Birkholzer and Q. Zhou, "Basin-scale hydrogeologic impacts of CO2 storage: capacity and regulatory implications," *International Journal of Greenhouse Gas Control*, vol. 3, no. 6, pp. 745–756, 2009.

[209] G. M. Ingram and J. L. Urai, "Top-seal leakage through faults and fractures: the role of mudrock properties," *Geological Society, London, Special Publications*, vol. 158, no. 1, pp. 125–135, 1999.

[210] C. Hermanrud and H. M. N. Bols, "Leakage from overpressured hydrocarbon reservoirs at Haltenbanken and in the northern North Sea," in *Norwegian Petroleum Society Special Publications*, pp. 221–231, Elsevier, 2002.

[211] R. H. Sibson, "Thickness of the seismic slip zone," *Bulletin of the Seismological Society of America*, vol. 93, no. 3, pp. 1169–1178, 2003.

[212] P. Teatini, N. Castelletto, and G. Gambolati, "3D geomechanical modeling for CO2 geological storage in faulted formations. A case study in an offshore northern Adriatic reservoir, Italy," *International Journal of Greenhouse Gas Control*, vol. 22, pp. 63–76, 2014.

[213] J. P. Verdon, "Significance for secure CO2 storage of earthquakes induced by fluid injection," *Environmental Research Letters*, vol. 9, no. 6, article 064022, 2014.

[214] Q. Zhou and J. T. Birkholzer, "On scale and magnitude of pressure build-up induced by large-scale geologic storage of CO2," *Greenhouse Gases: Science and Technology*, vol. 1, no. 1, pp. 11–20, 2011.

[215] J. E. Streit and R. R. Hillis, "Estimating fault stability and sustainable fluid pressures for underground storage of CO2 in porous rock," *Energy*, vol. 29, no. 9-10, pp. 1445–1456, 2004.

[216] C. Chen, J. Wan, W. Li, and Y. Song, "Water contact angles on quartz surfaces under supercritical CO2 sequestration conditions: experimental and molecular dynamics simulation studies," *International Journal of Greenhouse Gas Control*, vol. 42, pp. 655–665, 2015.

[217] A. J. Rinehart, T. A. Dewers, S. T. Broome, and P. Eichhubl, "Effects of CO2 on mechanical variability and constitutive behavior of the Lower Tuscaloosa Formation, Cranfield Injection Site, USA," *International Journal of Greenhouse Gas Control*, vol. 53, pp. 305–318, 2016.

[218] A. Fernandez and J. Santamarina, "Effect of cementation on the small-strain parameters of sands," *Canadian Geotechnical Journal*, vol. 38, no. 1, pp. 191–199, 2001.

[219] E. Bemer and J. Lombard, "From injectivity to integrity studies of CO2 geological storage-chemical alteration effects on carbonates petrophysical and geomechanical properties," *Oil & Gas Science and Technology–Revue de l'Institut Français du Pétrole*, vol. 65, no. 3, pp. 445–459, 2010.

[220] E. Bakker, S. J. Hangx, A. R. Niemeijer, and C. J. Spiers, "Frictional behaviour and transport properties of simulated fault gouges derived from a natural CO2 reservoir," *International Journal of Greenhouse Gas Control*, vol. 54, pp. 70–83, 2016.

[221] Z. Sun, D. N. Espinoza, and M. T. Balhoff, "Discrete element modeling of indentation tests to investigate mechanisms of CO2-related chemomechanical rock alteration," *Journal of Geophysical Research: Solid Earth*, vol. 121, no. 11, pp. 7867–7881, 2016.

[222] E. Liteanu, C. Spiers, and J. De Bresser, "The influence of water and supercritical CO2 on the failure behavior of chalk," *Tectonophysics*, vol. 599, pp. 157–169, 2013.

[223] S. Carroll, J. W. Carey, D. Dzombak et al., "Role of chemistry, mechanics, and transport on well integrity in CO2 storage environments," *International Journal of Greenhouse Gas Control*, vol. 49, pp. 149–160, 2016.

[224] I. Shovkun and D. N. Espinoza, "Coupled fluid flow-geomechanics simulation in stress-sensitive coal and shale reservoirs: impact of desorption-induced stresses, shear failure, and fines migration," *Fuel*, vol. 195, pp. 260–272, 2017.

[225] A. G. Ilgen, M. Aman, D. N. Espinoza et al., "Shale-brine-CO2 interactions and the long-term stability of carbonate-rich shale caprock," *International Journal of Greenhouse Gas Control*, vol. 78, pp. 244–253, 2018.

[226] J. Rutqvist, "The geomechanics of CO 2 storage in deep sedimentary formations," *Geotechnical and Geological Engineering*, vol. 30, no. 3, pp. 525–551, 2012.

[227] M. V. Madland, A. Finsnes, A. Alkafadgi, R. Risnes, and T. Austad, "The influence of CO2 gas and carbonate water on the mechanical stability of chalk," *Journal of Petroleum Science and Engineering*, vol. 51, no. 3-4, pp. 149–168, 2006.

[228] S. Farquhar, J. Pearce, G. Dawson et al., "A fresh approach to investigating CO2 storage: experimental CO2–water–rock interactions in a low-salinity reservoir system," *Chemical Geology*, vol. 399, pp. 98–122, 2015.

[229] Q.-Y. Liu, L. Tao, H.-Y. Zhu, Z. D. Lei, S. Jiang, and J. D. McLennan, "Macroscale mechanical and microscale structural changes in Chinese Wufeng shale with supercritical carbon dioxide fracturing," *SPE Journal*, vol. 23, no. 3, pp. 691–703, 2018.

[230] A. O. Olabode, *Diagenesis and Formation Stress in Fracture Conductivity of Shaly Rocks; Experimental-Modelling Approach in CO2-Rock Interactions*, Louisiana State University, 2017.

[231] Y. Ning, *Numerical Modeling and Simulations of Natural Gas Transport in Heterogeneous Shale Rocks Using the Lattice Boltzmann Method*, University of Houston, 2017.

[232] K. Bø, *Mobility Control for CO2 EOR in Heterogeneous Reservoirs*, The University of Bergen, 2014.

[233] S. Iglauer, C. Pentland, and A. Busch, "CO2 wettability of seal and reservoir rocks and the implications for carbon geosequestration," *Water Resources Research*, vol. 51, no. 1, pp. 729–774, 2015.

[234] W. Yu, H. R. Lashgari, K. Wu, and K. Sepehrnoori, "CO2 injection for enhanced oil recovery in Bakken tight oil reservoirs," *Fuel*, vol. 159, pp. 354–363, 2015.

[235] X. Zhang, J. Ge, F. Kamali, F. Othman, Y. Wang, and F. Le-Hussain, "Wettability of sandstone rocks and their mineral components during CO2 injection in aquifers: implications for fines migration," *Journal of Natural Gas Science and Engineering*, vol. 73, article 103050, 2020.

[236] B. Liu, C. Qi, X. Zhao et al., "Nanoscale two-phase flow of methane and water in shale inorganic matrix," *The Journal of Physical Chemistry C*, vol. 122, no. 46, pp. 26671–26679, 2018.

[237] S. Shahrokhabadi, T. D. Cao, and F. Vahedifard, "Thermo-hydro-mechanical modeling of unsaturated soils using isogeometric analysis: model development and application to strain localization simulation," *International Journal for Numerical and Analytical Methods in Geomechanics*, vol. 44, no. 2, pp. 261–292, 2020.

[238] R. Ershadnia, C. D. Wallace, and M. R. Soltanian, "CO_2 geological sequestration in heterogeneous binary media: Effects of geological and operational conditions," *Advances in Geo-Energy Research*, vol. 4, no. 4, pp. 392–405, 2020.

[239] J. Zhou, N. Hu, X. Xian et al., "Supercritical CO_2 fracking for enhanced shale gas recovery and CO_2 sequestration: Results, status and future challenges," *Advances in Geo-Energy Research*, vol. 3, no. 2, pp. 207–224, 2019.